University of Twente

EEMCS / Electrical Engineering
Robotics and *Mechatronics*

Real-time three-dimensional tracking and steering of flexible needles using two-dimensional ultrasound images

G.J. (Guus) Vrooijink

MSc Report

Committee:
Prof.dr.ir. S. Stramigioli
Dr. S. Misra
M. Abayazid, MSc
Dr.ir. F. van der Heijden

December 2012

Report nr. 034RAM2012
Robotics and Mechatronics
EE-Math-CS
University of Twente
P.O. Box 217
7500 AE Enschede
The Netherlands

Abstract

Needle insertion is one of the most commonly performed minimally invasive surgical procedures. Such needle insertions are often performed either for diagnosis (e.g., biopsy) or therapy (e.g., brachytherapy), both of which require accurate needle placement. Needle insertions are frequently performed under ultrasound image-guidance which provides visual feedback. Clinicians usually use rigid bevel-tipped needles that easily cut and penetrate the soft tissue. The steering capabilities of rigid bevel-tipped needles are limited. Thin and flexible bevel-tipped needles offer steering capabilities which allow the needle to be steered around sensitive organs and obstacles to reach a target. Accurate steering of a flexible needle in three-dimensional (3D) space is a demanding task which requires needle visualization during the insertion.

In this study, real-time 3D needle tip pose feedback is obtained by a novel technique which uses a two-dimensional (2D) ultrasound transducer. The 2D transducer is positioned at the needle tip, and orientated perpendicular to the direction of needle insertion. Position measurement of the needle tip in the out-of-plane direction of the transducer cannot be obtained directly. Therefore, the transducer needs to be repositioned at the needle tip during insertion, which is done by a positioning device. The required out-of-plane motion of the transducer is determined by the needle insertion velocity which is corrected by the tip velocities. Positioning of the transducer at the needle tip allows for computation of the tip pose, which is required for needle steering. Experiments show that maximum mean errors in needle tip positions are 0.64 mm, 0.25 mm and 0.27 mm along the insertion-, horizontal- and vertical-axes, respectively. The determined needle tip orientation errors are 2.68° and 2.83° about horizontal- and vertical-axes, respectively.

The needle tip pose is used in path planning in order to compute a needle trajectory to reach a desired target while avoiding an obstacle. The planner uses a customized Rapidly-exploring Random Trees (RRTs)-based path planner to determine feasible trajectories. The needle trajectory is determined by optimizing clinically motivated criteria in order to minimize tissue damage, or to maximize safety. The needle is controlled along such a trajectory by duty-cycled spinning of the needle during insertion. Experiments show needle steering with maximum targeting error of 3.5 mm (RMS) for the case with both a moving obstacle and target. Improved needle steering can be achieved by combining visualization with path planning and duty cycling, which offers the clinician an increase in targeting accuracy during minimally invasive procedures.

Acknowledgements

The successful completion of my project would not have been possible without the help of a number of people. First of all I would like to thank my thesis supervisor, Dr. Sarthak Misra, for giving me the opportunity to work on this project. During this project I gained a lot of interest in the fields of medical robotics, and was offered to continue working as a PhD student. I would also like to thank Momen Abayazid, for his flexibility, advice and feedback as my daily supervisor.

During my project great help was provided by the RAM technicians. I especially would like to thank Gerben te Riet o/g Scholten for helping with my practical problems and providing me with 3D printed components during my project. I would also like to thank the RAM secretary, Jolanda for helping out, in particular at the end of the project. During my project I had some very interesting (and amusing) discussions with my fellow graduate students, which I really appreciated. I would like to special thank my fellow graduate students Sander Janssen and Roel Metz: Sander for solving my C++ problems and Roel for helping with my mechanical design issues.

Last but not least I would also like to thank my family and girlfriend, Loes, for their support and faith during my graduation. I can very well imagine that I have been (pre)occupied with my graduation. So, thanks for that!, and for helping me when I most needed it.

— Guus Vrooijink

Contents

Introduction

During the last decade there has been a significant increase in Minimally Invasive Surgery (MIS). As research in the direction of MIS advances, more MIS technology becomes available for procedures. In MIS, the instrument is inserted into the body via a small incision allowing the clinician to perform a specific procedure. An example of MIS is percutaneous needle insertion. The needle punctures the skin and is used to perform a specific task at a specific location (Fig. 1). In Fig. 1(a), a breast biopsy

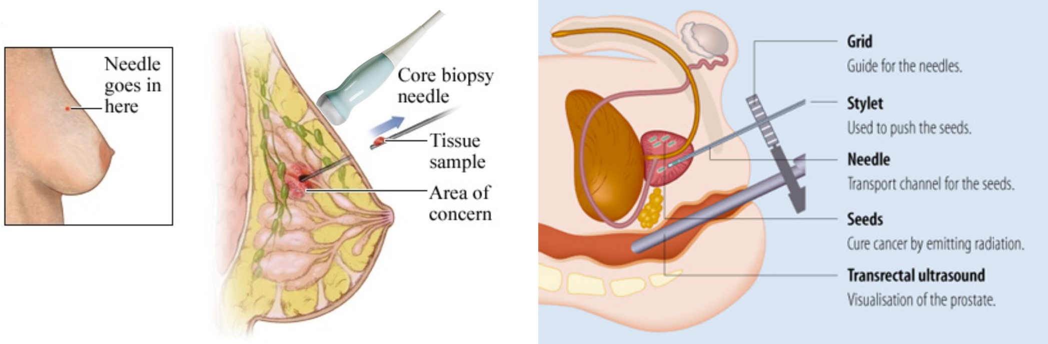

(a) (b)

Figure 1: Examples of minimally invasive surgical procedures. (a) A breast tissue biopsy, the needle is used to remove a small piece of tissue sample for diagnostic purposes (Healthwise Incorporate ©). (b) A prostate Brachytherapy procedure, the needle is used to insert an encapsulated radioactive seeds into the prostate, inside or next to the area requiring treatment (SeeDOS Ltd. ©)

is performed by inserting a needle. The needle is inserted to remove tissue for diagnoses. Needles are not only capable of tissue removal, they can also be employed to perform specialized treatment. In Fig. 1(b), brachytherapy is performed which implants multiple encapsulated radioactive seeds inside or near lesions tissue within the prostate. MIS has numerous advantages over traditionally open surgery, where large incisions are required to perform a specific task. MIS reduces patient trauma, scarring, risk at infection and results in shorter recovery time. But MIS has not only advantages, the clinician usually needs to rely on imaging modalities (e.g., computed tomography (CT) scans, fluoroscopy, magnetic resonance (MR) or ultrasound images) during procedure. Despite the various imaging modalities to visualize the needle, manual needle insertion remains a demanding task which requires extensive training. Even well trained and experienced clinicians are not always capable of reaching the target at once, therefore multiple insertion are required. Needle misplacement may result in misdiagnosis or unsuccessful treatment.

An alternative to manual needle insertion is robotic needle insertion (Fig. 2). Robotic steering of needles can be used to improve needle placement and to reduce the number of insertions required to reach the target. In order to steer the needle, a flexible bevel-tipped needle is used. During needle insertion, the asymmetric forces distributed at the needle tip, causing it to deflection in the direction of the bevel tip. By rotating the needle during insertion, its path can be controlled in order to steer the needle to reach a target.

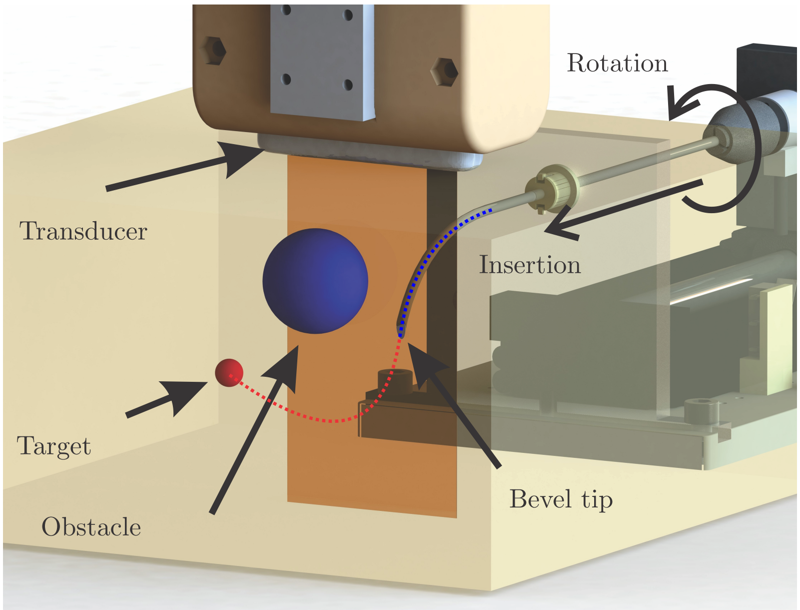

Figure 2: Illustration of needle steering. The needle is steered under ultrasound image-guidance using a needle insertion device. The needle is steered to reach a target while avoiding an obstacle.

Thesis Outline

The thesis is composed of three parts. The first part focuses on the design of a positioning device that is used to position the ultrasound transducer at the needle tip during insertion. Experiments are performed to evaluate the design specifications of the positioning device. The second part describes the three-dimensional (3D) tracking of flexible needles using two-dimensional (2D) ultrasound images. The positioning device designed in first part is used to position the ultrasound transducer to enable 3D needle tip tracking. Experiments are performed to evaluate the needle tip tracking accuracy. The third part presents the three-dimensional planning and steering of flexible needles. The proposed needle tip tracking method of part two is used to provide needle tip pose feedback used in path planning. The path planner determines the needle trajectory along which the needle is to be steered in order to reach a target while avoiding an obstacle. The thesis concludes with a conclusion on the work that was performed and provides recommendations for future work.

Thesis Contributions

[1] G.J. Vrooijink, M. Abayazid, S. Patil, R. Alterovitz and S. Misra, "Three-dimensional flexible needle steering using two-dimensional ultrasound images", In *Proceedings of the 4th Dutch Biomedical Engineering Conference*, Egmond aan Zee, The Netherlands, January 2013.

[2] G.J. Vrooijink, M. Abayazid, S. Misra, "Real-Time Three-Dimensional Flexible Needle Tracking using Two-Dimensional Ultrasound.", In *Proceedings of the IEEE International Conference on Robotics and Automation (ICRA)*, Karlsruhe, Germany, May 2013. (under review)

[3] G.J. Vrooijink, M. Abayazid, S. Patil, R. Alterovitz and S. Misra, "Three-Dimensional Needle Path Planning and Steering using Two-Dimensional Ultrasound Images", *The International Journal of Robotics Research.* (In Preparation)

[4] M. Abayazid, G.J. Vrooijink, S. Patil, R. Alterovitz and S. Misra, "Ultrasound-Guided Three-Dimensional Needle Path Planning and Steering", In *Proceedings of the IEEE Transactions on Robotics.* (In Preparation)

Part I

‘Ultrasound Transducer Positioning Device for Real-Time Three-Dimensional Flexible Needle Tracking’

Ultrasound Transducer Positioning Device for Real-Time Three-Dimensional Flexible Needle Tracking

Abstract— **Needle insertion is one of the most commonly performed minimally invasive procedures. Visualization of the needle during insertion is of great importance to perform a successful medical procedure. Improper or loss of visualization can cause the needle to be misplaced, which can result in misdiagnosis and delayed or unsuccessful treatment. Positioning the ultrasound transducer at a desired location to provide proper visual feedback is a demanding task. This work presents a device capable of real-time positioning the ultrasound transducer in three-dimensional space at the needle tip location during procedures. Experiments are performed to evaluate velocity control of the device. Results show that a robotic positioning device is developed according to requirements for ultrasound-guided needle tracking. This study presents a positioning device to accurate position the ultrasound transducer and thereby improve needle visualization during medical procedures.**

I. INTRODUCTION

One of the most commonly performed minimally invasive procedures is needle insertion. Proper visualization of the needle is of great importance for either successful diagnosis (e.g., biopsies) or therapy (e.g., brachytherapy). Improper needle visualization can cause needle misplacement, which can result in misdiagnosis and delayed or unsuccessful treatment [1], [2]. Percutaneous interventions involving needles are often performed under image-guidance, including computed tomography (CT) scans, fluoroscopy, magnetic resonance (MR) or ultrasound imaging. Some of these techniques have drawbacks, where CT scans expose the patient to high doses of radiation, and MR-guided procedures are incompatible with magnetic objects [3], [4]. Ultrasound is a commonly used imaging modality to visualize the needle and target during procedure, which is proven to be accessible and safe to use [5], [6].

The ultrasound transducer must be proper positioned to provide the clinician with feedback of the needle or target location. Proper positioning of the ultrasound transducer at the desired location is a demanding task. Several studies show the use robotic devices performing the positioning task of the ultrasound transducer. The use of a robot which enables ultrasound transducer positioning via shared control between clinician and image processing has been documented by [7]. In literature, robotic devices are also reported to enable carotid artery or target motion tracking by [8], [9], respectively. Other studies use robotic devices to construct a volume from 2D ultrasound images [10], [11]. Neshat and Patel used 2D ultrasound to construct a volume along the needle shaft, which is used to track flexible needles in real-time [12]. However, the volume size remains a compromise between its size and acquisition time, which is limited in real-time applications. A method for real-time 3D flexible needle tip tracking is to place the ultrasound transducer perpendicular with respect to the needle insertion direction. During needle insertion, the transducer needs to be repositioned by a device that compensates for movement in the out-of-plane direction. Therefore, this method requires a positioning device that enables compensation for needle tip motion during insertion.

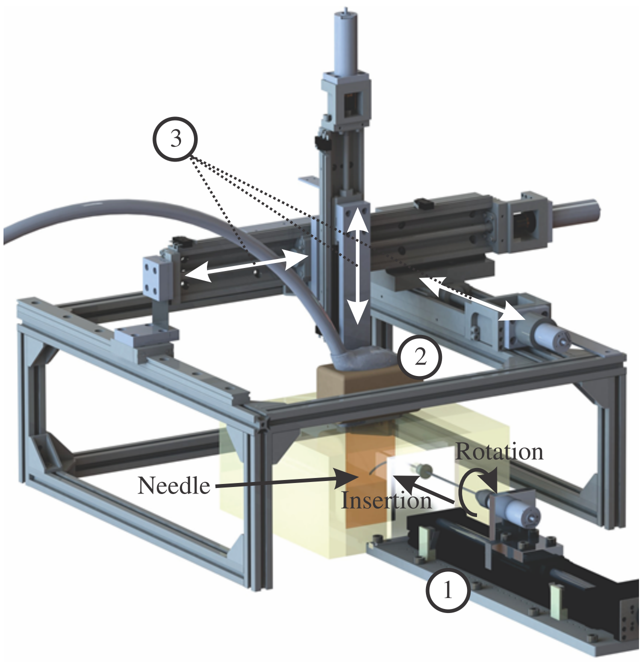

Fig. 1. A flexible needle with a bevel tip is inserted in the soft-tissue simulant by a needle insertion device (NID) ①. Depending on the orientation of the bevel tip, the needle can deflect in the three-dimensional space. An ultrasound transducer ② is used to track the needle tip, which is placed perpendicular to the needle insertion direction. The ultrasound transducer is repositioned by a positioning device along ③ at the needle tip during needle insertion.

Therefore this paper presents a positioning device that enables the perpendicular placed ultrasound transducer to move according the needle tip motion. The positioning device allows translational motions in 3D, which can be controlled in both position and velocity.

The paper is organized as follows: Section II describes

This work was supported by funds from the Netherlands Organization for Scientific Research (NWO).

requirements for the positioning device, its design and fabrication. Section III, the experiments performed to evaluate the velocity control of the positioning device. Section IV, a conclusion and directions for future work is provided.

II. Design and Fabrication

This section describes the design and fabrication of the ultrasound transducer positioning device. First, the problem analysis is performed and requirements are determined. A design was made in order to fulfill all requirements. Finally, the fabrication of the positioning device is presented.

A. Problem Analysis

The main function of the of the positioning device is to position the ultrasound transducer in order to visualize the needle tip during insertion. The 2D ultrasound transducer needs to be positioned along all axes of a 3D environment allowing it to track the needle tip over a horizontal surface (e.g., cubic shaped soft-tissue simulant). The positioning device will mainly be used to track the needle tip in 3D by holding a perpendicular orientated ultrasound transducer. However, the design should consider further development. Further development could be needle tracking in a traditional manner, whereby the image plane of the transducer is placed along the needle shaft to visualize the needle shape. Other developments could be tracking of target or obstacle motion. Most likely more degrees of freedom (DOF) will be added to the device. For instance, rotation of the transducer allows the needle, target or obstacle to be tracked over curved surfaces. Besides further development, the needle insertion device (NID) design specifications should be considered. [13]. The positioning device will generally be used in combination with the NID, which makes it important to match specifications. These specifications are, needle insertion velocity and insertion depth, as well for the allowed soft-tissue simulant size.

The ultrasound transducer which is orientated perpendicular to the needle insertion axis (Fig. 2) provides a radial cross-sectional view of the needle. The images are acquired at a frequency of 25 Hz (image every 40 ms) using a Siemens Acuson S2000 ultrasound machine (Siemens AG, Erlangen, Germany). The ultrasound machine is linked to a computer via S-video capturing device which transfers the images (720×576 pixels) with an effective resolution of 0.12 mm/pixel. The transducer must be located along the insertion axis at the needle tip during insertion to determine the needle tip position. The needle tip will initially move in the insertion direction, but deflection occurs due to the asymmetric distributed force at the bevel-tip. Compensation for the out-of-plane motion of the needle tip is required to obtain the needle tip position during insertion. In order to determine the required out-of-plane motion of the transducer, the needle insertion velocity is corrected by tip velocities (in-plane needle tip deflection). The transducer needs to be accelerated when the needle tip enters the ultrasound image plane in order to catch up with the needle tip motion. Needle insertion velocities up to 20 mm/s are considered.

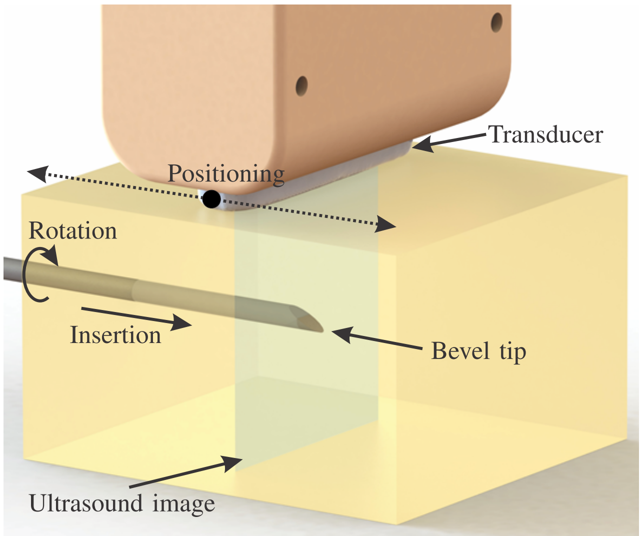

Fig. 2. A flexible bevel-tipped needle is inserted in the soft-tissue simulant. During insertion the needle deflects along a curved trajectory in the direction of the bevel-tip. An two-dimensional ultrasound transducer is placed perpendicular to the needle insertion-axis. The transducer is relocated along the insertion-axis at the needle tip during insertion to provide visual feedback.

The transducer position can be described by,

$$x(t) = x_0 + v_0 t + \frac{1}{2} a_{max} t^2, \tag{1}$$

where a_{max} represent the acceleration of the transducer, and x_0 and v_0 its initial position and velocity, respectively. The initial position and velocity of the transducer equals zero. Hence, the required transducer acceleration a_{max} can be computed according,

$$a_{max} = \frac{2x(t)}{t^2}. \tag{2}$$

The time between images is known to be 40 ms, and the needle insertion velocity to be 20 mm/s. During this period of time, the needle tip travels a distance of 0.8 mm. Thus, the required acceleration of the transducer can be computed according (2), which is determined at 1 m/s^2.

1) Requirements: The design requirements of the ultrasound transducer positioning device are provided in Table I. The span describes the positioning reach of the ultrasound transducer, which should cover the entire surface of the largest cubical-shaped soft-tissue simulants used. The velocity of the ultrasound transducer should be larger than the needle insertion velocity. Although, it is desirable that initial positioning of the ultrasound transducer is done at high velocities. In order to catch up with the needle tip, the transducer needs to be accelerated. The required acceleration ensures that the stationary transducer is moved such that subsequent ultrasound image is taken at the needle tip. The positioning accuracy should be less than the mm per pixel resolution of the ultrasound images to provide sub-pixel accuracy.

TABLE I

THE POSITIONING DEVICE DESIGN REQUIREMENTS: THE TOTAL SPAN, VELOCITY, ACCELERATION AND POSITIONING ACCURACY OF THE ULTRASOUND TRANSDUCER ALONG THE x-, y- AND z-AXES.

Requirement	x-axis	y-axis	z-axis
Span	200 mm	200 mm	50 mm
Velocity	$\gg 20$ mm/s	$\gg 20$ mm/s	$\gg 20$ mm/s
Acceleration	1 m/s^2	1 m/s^2	1 m/s^2
Positioning Accuracy	< 0.12 mm	< 0.12 mm	< 0.12 mm

(a) (b) (c)

Fig. 3. Positioning devices: (a) Robotic arm, (b) Delta robot and (c) Cartesian robot

2) Considerations: In order to use the positioning device in the existing setup, several design considerations should be made. In terms of safety, the whereabouts of the robotic positioning device should be bounded to a specific working area. The working area is limited by a frame which surrounds the setup, which is used to mount the auxiliary-hardware (e.g., CCD cameras and light sources) used for experiments. The existing setup uses calibrated stereo cameras, which should preferable not be removed during operation of the positioning device. It is allowed that the camera view is obstructed when the positioning device is used. Further, in order to provide consistent measurements, a clamp should be developed which holds the ultrasound transducer in a fixed pose.

B. Design

Several robotic positioning devices are considered, including robotic arms with sufficient degrees of freedom (DOF), delta robots and Cartesian robots in Fig. 3(a), (b) and (c), respectively. All devices are capable of accurately position the ultrasound transducer at the needle tip during needle insertion. Although, the size and large reach of the industrialized robotic arm, combined with the limited working area of the setup, introduces potential safety issues. Further, the delta robot which should be mounted above the soft-tissue simulant conflicts with the mounted camera in the existing setup. In order to use the setup for various experiments, the exchange between delta robot and camera is required. The exchange of devices consumes conversion time and might require re-calibration for every experiment. The use of a Cartesian robot can be well integrated in the existing setup. The reach of the Cartesian robot is well known and can be configured such that it does not conflict with the existing hardware. Further, the Cartesian robot can be positioned outside the view of the cameras such that various experiments

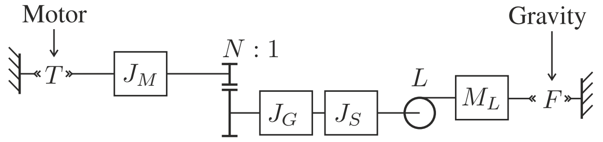

Fig. 4. The Ideal Physical Model (IPM) of a linear stage, including motor, gear head, lead screw, load mass and the loads gravitational force. T represents the torque delivered by the electric motor, while F describes the gravitational force acting on the load mass (M_L). Further, J_M, J_G and J_S describe the inertias of the motor, gear head and lead spindle, respectively. N describes the gear head reduction ratio, while L describes the lead (pitch) of the lead screw.

TABLE II

THE LEAD SPINDLE AND LOAD PARAMETERS. J_S REPRESENTS THE SPINDLE INERTIA, WHILE L DESCRIBES THE LEAD OF THE SPINDLE. THE POSITIONING ACCURACY IS GIVEN BY ϵ. THE STARTING TORQUE OF THE LINEAR STAGE IS DESCRIBED BY T_F. THE DRIVEN LOAD IS DENOTED BY M_L.

	x-axis	y-axis	z-axis
J_S [kgm^2]	$5.65 \cdot 10^{-6}$	$2.23 \cdot 10^{-6}$	$0.63 \cdot 10^{-6}$
L [mm]	5	5	5
ϵ [mm]	0.0076	0.0072	0.0077
T_F [mNm]	40.0	20.0	12.0
M_L [kg]	10.0	6.0	3.0

can be performed without additional conversion time and recalibration. Therefore, a Cartesian robotic device is designed according to design requirements and considerations. Three linear stages are orthogonally mounted on top of each other to position the ultrasound transducer in 3D (Fig. 1). The first linear stage (x-axis) and a passive guide are positioned parallel to the needle insertion direction. A second linear stage (y-axis) is used to span the distance between the first linear stage and the passive guide. The passive guide is used to support the weight of second linear stage, which prevents it from sagging. A leaf spring system connects the passive guide with the second linear stage. The leaf spring system is used relax the constraint on parallelism between the first stage and passive guide. The third linear stage (z-axis) is mounted on top of the second linear stage which completes the 3 DOF positioning device.

1) Motor Calculations: In order to actuate the linear stages, calculations must be performed to determine the required motor and gear head specifications. An Ideal Physical Model (IPM) which describes a single linear stage is presented in Fig. 4. Prior knowledge about the parameters can be found in Table II. The desired load force can be computed by,

$$F_L = m_L a_{max} + m_L g, \tag{3}$$

where a_{max} represents the constant acceleration of the ultrasound transducer according to (2), and g the gravitational acceleration. The gravitational acceleration only affects the z-axis, hence the gravitational force $m_L g$ equals zero in x- and y-axes. Since there is no prior information on the gear head and motor, we initially choose the gear head transmission ratio N equal to 1, and assume zero gear head and motor inertia. Later will be shown that these assumptions

TABLE III

THE MOTOR SPECIFICATIONS: P DESCRIBES THE ELECTRIC MOTOR POWER. J_M REPRESENTS THE MOTOR INERTIA, WHILE V_{nom} DESCRIBES THE NOMINAL VELOCITY UNDER NOMINAL LOAD. THE NOMINAL AND STALL TORQUES ARE DENOTED BY T_{nom} AND T_{stall}, RESPECTIVELY.

	x-axis	y-axis	z-axis
P [W]	25	12	12
J_M [kgm^2]	$0.445 \cdot 10^{-6}$	$0.225 \cdot 10^{-6}$	$0.225 \cdot 10^{-6}$
V_{nom} [rpm]	10400	12100	12100
T_{nom} [mNm]	22.5	10.8	10.8
T_{stall} [mNm]	121.0	35.1	35.1

TABLE IV

THE GEAR HEAD SPECIFICATIONS: N DESCRIBES THE TRANSMISSION RATIO. THE BACKLASH AT THE OUTPUT SHAFT OF THE GEAR HEAD IS DESCRIBED BY B. J_G REPRESENTS THE GEAR HEAD INERTIA. T_{con} DESCRIBES THE MAXIMUM CONTINUOUS TORQUE, WHILE T_{ip} DESCRIBES THE INTERMITTENT PERMISSIBLE TORQUE AT THE OUTPUT. THE GEAR HEAD EFFICIENCY IS DENOTED BY η.

	x-axis	y-axis	z-axis
N	$4.8:1$	$5.4:1$	$14:1$
B [°]	0.7	1.0	1.2
J_G [kgm^2]	$0.15 \cdot 10^{-6}$	$0.05 \cdot 10^{-6}$	$0.04 \cdot 10^{-6}$
T_{con} [Nm]	1.00	0.50	0.60
T_{ip} [Nm]	1.25	0.80	0.90
η [%]	80	84	70

can be made. Further, since there is also no prior knowledge on the dynamic friction, the starting torque T_F is assumed to be equal to the dynamic friction. The required angular acceleration of the motor is then given by,

$$\ddot{\phi}_m = \frac{2\pi}{L} a_{max}, \tag{4}$$

which can be used to determine the initial required motor torque,

$$T_{init} = \ddot{\phi}_m J_S + \frac{L}{2\pi} F_L + T_F. \tag{5}$$

From (5) the following values for T_{init} are calculated: 55.1 mNm, 27.6 mNm, and 38.6 mNm for the linear stages of x-, y- and z-axes, respectively. By using the computed values for T_{init}, the motors and gear heads combinations are chosen ((Table III) and (Table IV), repectively). In order to evaluate if the earlier made assumptions do not conflict with the selected motor gear head combinations, the required motor torque can be computed with all known parameters,

$$T = N\ddot{\phi}_m J_M + \frac{1}{\eta N}(\ddot{\phi}_m J_G + T_{init}), \tag{6}$$

which equal 14.2 mNm, 6.6 mNm and 6.7 mNm for the linear stages of x-, y- and z-axes, respectively. The computed motor torques T are within the specifications of selected motors (Table (III)). Thus, the assumptions could be made in order to determine the motor and gear head combinations. Further, the load velocities (V_L) can be computed according to,

$$V_L = \frac{V_{nom}}{60} \frac{L}{N}, \tag{7}$$

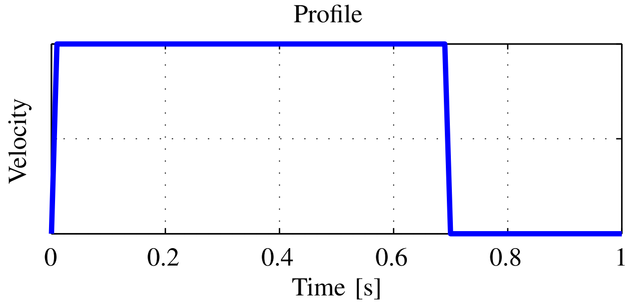

Fig. 5. The velocity profile applied to evaluate velocity control. A velocity step is applied to evaluate acceleration, deceleration (negative acceleration) and the referenced velocity.

which equals 181, 186 and 72 mm/s (x-, y- and z-linear stages, respectively). Thus, it is shown that the computed load velocities satisfy the requirements of Table I.

C. Fabrication

The positioning device is fabricated by three orthogonally-placed translational stages LX30, LX26 and LX20 (Misumi Group Inc., Tokyo, Japan). The three translational stages enable movement with an effective span of, 206 mm, 173 mm, and 73 mm in x-, y- and z-axes, respectively. Each stage is actuated by an ECMax22 motor (Table III) with a GP32/22 gear head (Table IV) (Maxon Motor, Sachseln, Switzerland), which is velocity controlled by an Elmo Whistle 2.5/60 motor controller (Elmo Motion Control Ltd, Petach-Tikva, Israel). The positioning accuracy of the linear stages are given in Table II. If we assume torsional stiffness of the gear head, the positioning accuracy of the gear head could be determined from the gear backlash (Table IV). By combining the inaccuracies introduced by the linear stage and the gear head, the positioning accuracy of the complete positioning device can be determined. The positioning accuracy of the positioning device is determined at 27 μm, 35 μm and 41 μm along the x-, y- and z-axes, respectively. In order to provide consistent measurements, the ultrasound transducer is clamped at the end-effector in a fixed pose using a special designed clamp. A 3D scan of the ultrasound transducer was made using a Vivid 910 3D laser scanner (Konica Minolta Sensing, Inc., Tokyo, Japan). The 3D scan is used to design a transducer clamp capable of fixing the transducer in a fixed pose at end-effector of the positioning device. The designed clamp is 3D printed using a Eden 250 3D printer (Objet Ltd., Rehovot, Israel) and mounted at the positioning device end-effector.

III. EXPERIMENTS

In this section, the positioning device used to position the ultrasound transducer is evaluated. In order to evaluate the performance of the positioning device, experiments are performed and corresponding results presented and discussed.

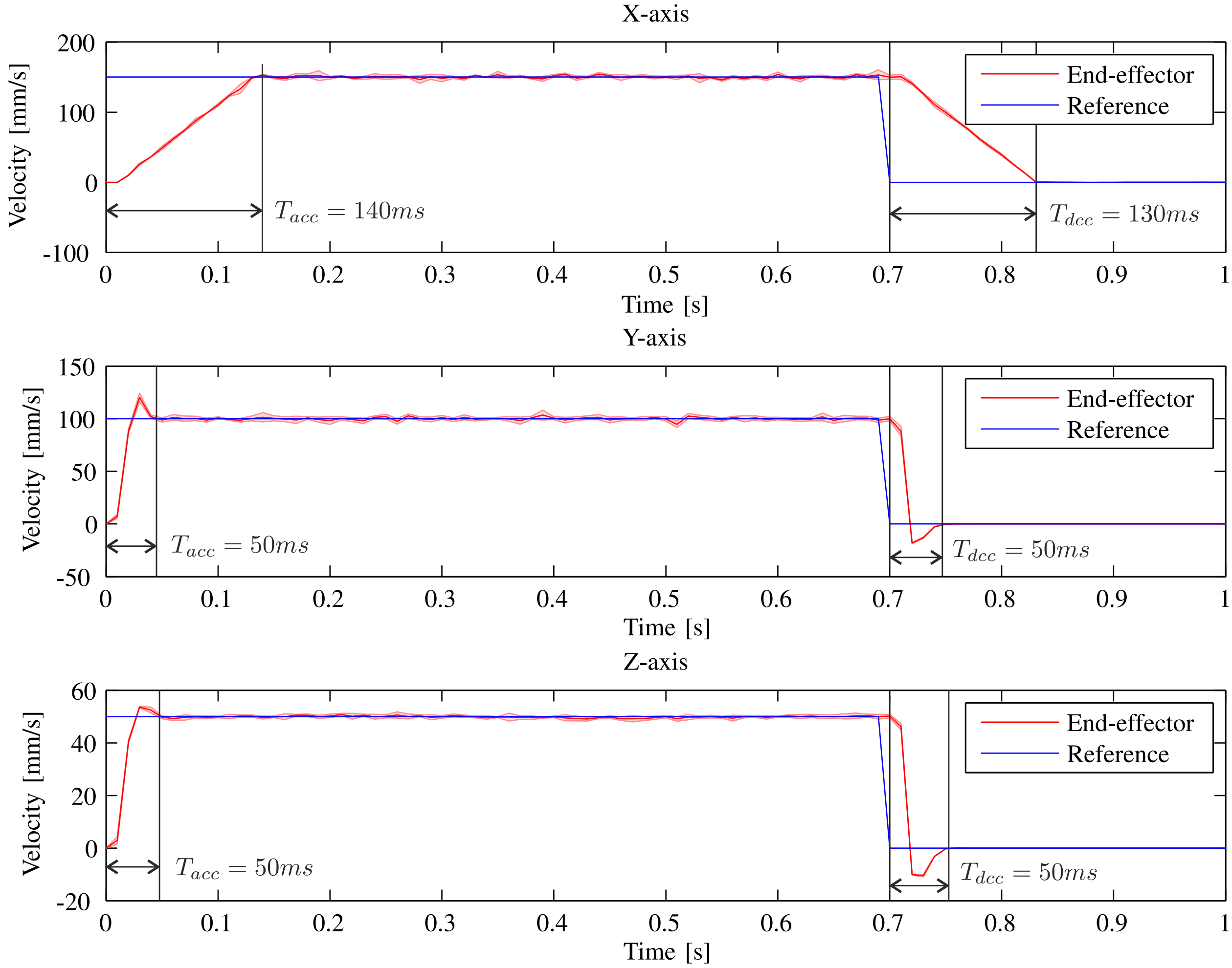

Fig. 6. The velocity responses to the applied velocity profiles (Fig. 5). T_{acc} describes the time to accelerate to reach the required velocity, while T_{dcc} describes the time to decelerate to zero velocity.

A. Experimental plan

The positioning device enables movement of the ultrasound transducer along x-, y- and z-axes. The motion of the stages are velocity controlled. In order to evaluate the requirements of Table I, a velocity profile is applied (Fig. 5). The velocity step sizes are chosen, 150, 100 and 50 mm/s in x-, y- and z-axes, respectively.

B. Results and Discussion

The responses to the velocity profiles can be found in Fig. 6. From the results in Fig. 6, acceleration times of 140 ms, 50 ms and 50 ms can be observed in x-, y- and z-axes, respectively. The corresponding accelerations are 1071 mm/s^2, 2000 mm/s^2 and 2000 mm/s^2. From these results can be concluded that the specifications of Table I are met. Further, the decelerations times are determined at 130 ms, 50 ms and 50 ms in x-, y- and z-axes, respectively. The corresponding decelerations are 1154 mm/s^2, 2000 mm/s^2 and 2000 mm/s^2, which also satisfy the requirements. It is shown that the velocity step sizes of 150 mm/s, 100 mm/s and 50 mm/s are reached, which also consents the requirements.

IV. Conclusions and Future Work

Experiments are performed to evaluate velocity control of the ultrasound positioning device. Results show that a robotic positioning device is constructed according the requirements for ultrasound-guided needle tracking (Table I). Therefore, this study presents a positioning device capable of accurate positioning the ultrasound transducer and thereby improves needle visualization during medical procedures.

For future work, we will add more DOF to the positioning device. More DOF allows for ultrasound needle tip tracking and target motion tracking over curved surfaces. The additional degrees of freedom provides tracking in more clinically relevant scenarios.

References

[1] J. H. Youk, E.-K. Kim, M. J. Kim, J. Y. Lee, and K. K. Oh, "Missed breast cancers at us-guided core needle biopsy: How to reduce them," *Radiographics*, vol. 27, no. 1, pp. 79–94, 2007.

[2] S. Nag, W. Bice, K. DeWyngaert, B. Prestidge, R. Stock, and Y. Yu, "The american brachytherapy society recommendations for permanent prostate brachytherapy postimplant dosimetric analysis," *International Journal of Radiation Oncology Biology Physics*, vol. 46, no. 1, pp. 221–230, 2000.

[3] S. G. Shulman and D. E. March, "Ultrasound-guided breast interventions: Accuracy of biopsy techniques and applications in patient management," *Seminars in Ultrasound, CT, and MRI*, vol. 27, no. 4, pp. 298–307, 2006.

[4] Y.-C. Wu, D.-R. Chen, and S.-J. Kuo, "Personal experience of ultrasound-guided 14-gauge core biopsy of breast tumor," *European Journal of Surgical Oncology (EJSO)*, vol. 32, no. 7, pp. 715–718, 2006.

[5] N. Abolhassani, R. Patel, and M. Moallem, "Needle insertion into soft tissue: A survey," *Medical Engineering and Physics*, vol. 29, no. 4, pp. 413–431, 2007.

[6] J. op den Buijs, M. Abayazid, C. L. de Korte, and S. Misra, "Target motion predictions for pre-operative planning during needle-based interventions," in *Proceedings of the IEEE International Conference on Engineering in Medicine and Biology Society (EMBC)*, pp. 5380–5385, Boston, USA, August 2011.

[7] S. Salcudean, G. Bell, S. Bachmann, W. Zhu, P. Abolmaesumi, and P. Lawrence, "Robot-assisted diagnostic ultrasound - design and feasibility experiments," in *Medical Image Computing and Computer-Assisted Intervention (MICCAI)* (C. Taylor and A. Colchester, eds.), vol. 1679 of *Lecture Notes in Computer Science*, pp. 1062–1071, Springer Berlin / Heidelberg, 1999.

[8] R. Nakadate, J. Solis, A. Takanishi, E. Minagawa, M. Sugawara, and K. Niki, "Out-of-plane visual servoing method for tracking the carotid artery with a robot-assisted ultrasound diagnostic system," in *Proceedings of the IEEE International Conference on Robotics and Automation (ICRA)*, pp. 5267 –5272, Shanghai, China, may 2011.

[9] C. Nadeau and A. Krupa, "Intensity-based direct visual servoing of an ultrasound probe," in *Proceedings of the IEEE International Conference on Robotics and Automation (ICRA)*, pp. 5677–5682, Shanghai, China, May 2011.

[10] E. M. Boctor, P. Stolka, H.-J. Kang, C. Clarke, C. Rucker, J. Croom, E. C. Burdette, and R. J. Webster III, "Precisely shaped acoustic ablation of tumors utilizing steerable needle and 3d ultrasound image guidance," vol. 7625, pp. 76252N–76252N–10, 2010.

[11] M.-A. Janvier, L.-G. Durand, M.-H. R. Cardinal, I. Renaud, B. Chayer, P. Bigras, J. de Guise, G. Soulez, and G. Cloutier, "Performance evaluation of a medical robotic 3d-ultrasound imaging system," *Medical Image Analysis*, vol. 12, no. 3, pp. 275–290, 2008.

[12] H. Neshat and R. Patel, "Real-time parametric curved needle segmentation in 3d ultrasound images," in *Proceedings of the IEEE RAS EMBS International Conference on Biomedical Robotics and Biomechatronics (BioRob)*, pp. 670–675, Scottsdale, USA, October 2008.

[13] Y. Veen, "Needle and soft tissue: experimental design and observations," master's degree in mechanical engineering - biomechanical engineering, University of Twente, june 2011.

Part II

‘Real-Time Three-Dimensional Flexible Needle Tracking using Two-Dimensional Ultrasound’

Real-Time Three-Dimensional Flexible Needle Tracking using Two-Dimensional Ultrasound

Gustaaf J. Vrooijink, Momen Abayazid and Sarthak Misra
University of Twente, The Netherlands

***Abstract*— Needle insertion is one of the most commonly performed minimally invasive procedures. Visualization of the needle during insertion is key for either successful diagnosis or therapy. This work presents the real-time three-dimensional tracking of flexible needles during insertion into a soft-tissue simulant using a two-dimensional ultrasound transducer. The transducer is placed perpendicular to the needle tip to measure its position. During insertion the transducer is robotically repositioned to track the needle tip. Positioning of the transducer is accomplished via an estimator, that uses the needle insertion velocity corrected by needle tip velocities to estimate out-of-plane motion. Experiments are performed to validate the needle tip pose during tracking. The maximum mean errors in needle tip position along the x-, y- and z-axes are 0.64 mm, 0.25 mm and 0.27 mm, respectively. The error in tip orientations (θ-about the y-axis and ϕ-about the z-axis) are 2.68° and 2.83°, respectively. This study demonstrates the feasibility to use needle tip pose feedback to robotically steer needles, and thereby improve accuracy of medical procedures.**

I. INTRODUCTION

In numerous minimally invasive medical procedures needles are inserted into tissue either for diagnosis or therapy. The success of the procedure depends on needle placement accuracy. Needle misplacement can cause misdiagnosis (e.g., biopsies) and delayed or unsuccessful treatment (e.g., brachytherapy) [1], [2]. Needle insertion is often performed under image-guidance, e.g., computed tomography (CT) scans, fluoroscopy, magnetic resonance (MR) or ultrasound images. Using CT has drawbacks, as the patient is exposed to high doses of radiation during the procedure [3]. MR-guided procedures can only be combined with instruments made of nonmagnetic and dielectric materials [4]. Ultrasound is proven to be a safe and an accessible imaging technique to visualize both the needle and target (lesion) during the procedure [5], [6].

During such procedures, rigid needles give the clinician limited steering capabilities to compensate for target motion, and initial misalignment between the needle and target. Recent studies show methods to deal with the mentioned problems, which involve pre-operative planning, target motion compensation and robot-controlled insertions [7]–[10]. Flexible needles with asymmetric (e.g., bevel) tips can be steered to compensate for target motion and initial misalignment. Further, this enables the capability to avoid sensitive organs (e.g., blood vessels) and obstacles (e.g., bones). For all these capabilities the needle needs to be accurately controlled. Robotic needle insertion devices have been used in previous studies to improve the needle placement accuracy [10]–[15]. Some of these studies use two-dimensional (2D) ultrasound to assist the robotically inserted needles, but movement is limited to the 2D image plane [10], [12]. Neshat and Patel used real-time 2D ultrasound images to construct a volume in which curved needles are tracked [16]. However, the volume remains a compromise between its size and acquisition time. Tracking surgical instruments such as cardiac catheters using three-dimensional (3D) ultrasound images has also been demonstrated [17], [18]. However, the 3-8 mm diameter of these cardiac catheters (some equipped with markers) are significantly larger than the diameter (0.5-1.0 mm) of flexible needles. Therefore, the cardiac catheters will result in a more detailed reproduction than a flexible needle. Modern 3D ultrasound transducers available for real-time applications have a limited voxel resolution. Low voxel resolutions of 3D ultrasound limits accurate needle tip detection up to 3 mm [19]. Nadeau and Krupa described target motion tracking with 2D ultrasound [20], but the allowed target motion was limited. No available studies to date describe real-time 3D tracking of flexible needles inserted into soft-

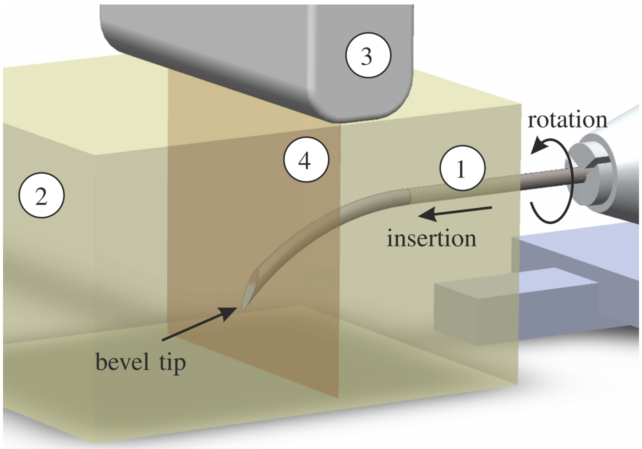

Fig. 1. A flexible needle 1 with a bevel tip is inserted in the soft-tissue simulant 2. Depending on the orientation of the bevel tip, the needle can deflect in the three-dimensional space. The needle tip is tracked by an ultrasound transducer 3, which is placed perpendicular to the needle insertion direction. The two-dimensional ultrasound image plane 4 provides a radial cross-sectional view of the needle. During insertion the ultrasound transducer is robotically repositioned to track the needle tip in real-time.

This work was supported by funds from the Netherlands Organization for Scientific Research (NWO).

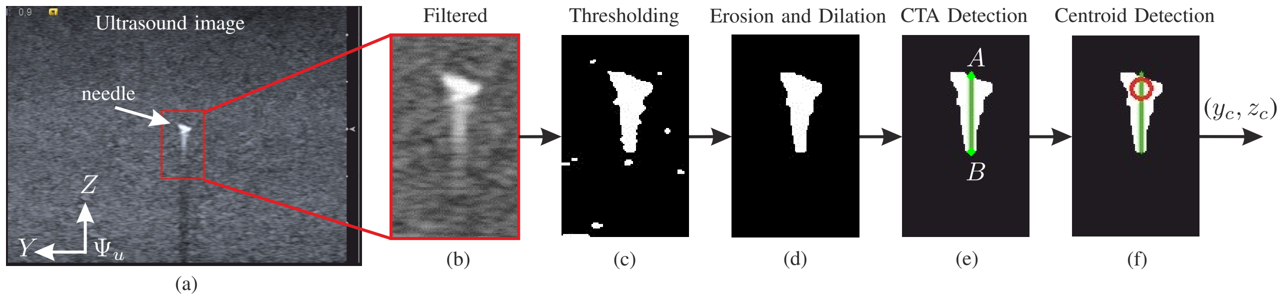

Fig. 2. Image processing methodology to determine the needle centroid location (y_c,z_c) in the ultrasound images. (a) The ultrasound input image is a radial cross-sectional view of the needle with the comet tail artifact (CTA). (b) In order to minimize speckle in the ultrasound image, a median filter is applied to the needle with the CTA. (c) A binary image is obtained by thresholding. (d) The remaining speckle in the image is removed by erosion and dilation. (e) A line detection algorithm using Hough transform is applied to detect the needle with the CTA. This line is denoted $\overline{AB}$. (f) In $\overline{AB}$, A represents the needle surface. The needle centroid (y_c, z_c) is evaluated as the center of the red circle (since the diameter of the needle is known).

tissue. This paper presents a novel technique to track flexible needles in 3D using a 2D ultrasound transducer. The 2D ultrasound transducer is placed perpendicular with respect to the needle insertion direction (Fig. 1). The transducer is unable to measure needle tip movement in its out-of-plane direction directly. Therefore, an estimator is used to evaluate the out-of-plane motion. The transducer is then repositioned by a positioning device to compensate for movement in the out-of-plane direction. This enables 3D real-time tracking of the needle tip through the soft-tissue simulant.

The paper is organized as follows: Section II describes the image processing algorithm used to detect the needle tip location from 2D ultrasound images. Further, computation of the needle tip pose, and the image-guided motion controller used for repositioning of the ultrasound transducer during insertion are discussed. Section III describes the setup and experiments performed to validate the performance of the needle tip tracking system, and results are also presented. Finally in Section IV, we conclude and provide directions for future work.

II. METHODS

This section presents a method to track the needle tip in 3D by using a 2D ultrasound transducer. First, image processing to locate the needle in ultrasound images is described. Subsequently, computations required to determine the needle tip pose are explained. Finally, the controller which positions the ultrasound transducer at the needle tip is presented.

A. Ultrasound Image Processing

Needle tip position feedback for control is provided by ultrasound image processing. The ultrasound transducer is placed perpendicular to the needle insertion direction (Fig. 1). The images show a 2D radial cross-sectional view of the needle, which has ideally a circular shape. However the circular shape is deformed by the reverberation artifact as shown in Fig. 2(a) [21]. Reverberation occurs when sound waves are repeatedly reflected between different boundaries, that are introduced by differences in acoustic impedances between materials. The acoustic impedance difference between needle and soft tissue is significant. The impedance difference results in multiple and strong bouncing echoes in the needle before returning to the transducer, which causes the artifact. The resulting artifact which has a tail-shaped structure in images of equally spaced echoes along the ultrasound wave is often referred to as the comet tail artifact (CTA) [22]. The length of the tail-shaped structure depends on the echoes that are received by the transducer.

An image processing algorithm is developed to determine the location of the needle, which is affected by the CTA (Fig. 2). Ultrasound images with a radial cross-sectional view of the needle are used. The needle visibility is enhanced, and speckling is removed by applying basic image processing techniques such as, median filtering, thresholding, and erosion and dilation in Fig. 2(b), (c) and (d), respectively. A line detection algorithm based on Hough transform is used to find a set of vertical line segments describing the needle with the CTA. Each line segment must be at least the length of the needle diameter. We assume that the needle has a symmetric shape along the ultrasound sound wave (z-axis of frame (Ψ_u) in Fig. 2). By using both the symmetry property and the set of vertical line segments, a mean line segment ($\overline{AB}$) describing the needle with the CTA is determined (Fig. 2(e)). Changes in the length of the tail-shaped structure of the CTA will affect the mean line segment at B. The mean line segment at A represents a point on the surface of the needle. The needle centroid (y_c, z_c) is located on $\overline{AB}$, at a distance equal to the radius of the needle from A (Fig. 2(f)). If the transducer is properly positioned at the needle tip, the centroid (y_c, z_c) can be used to compute the needle tip pose.

B. Needle Tip Pose Computation

An overview of the various coordinate systems required to compute the needle tip pose are provided in Fig. 3. The needle is inserted with velocity ($\mathbf{v}_i$) along the x-axis in the soft-tissue simulant by the needle insertion device (NID). In order to provide feedback, the needle tip position expressed in the fixed reference frame (Ψ_0) given by,

$$\mathbf{p}_t^0 = \begin{bmatrix} p_x & p_y & p_z \end{bmatrix}^T, \tag{1}$$

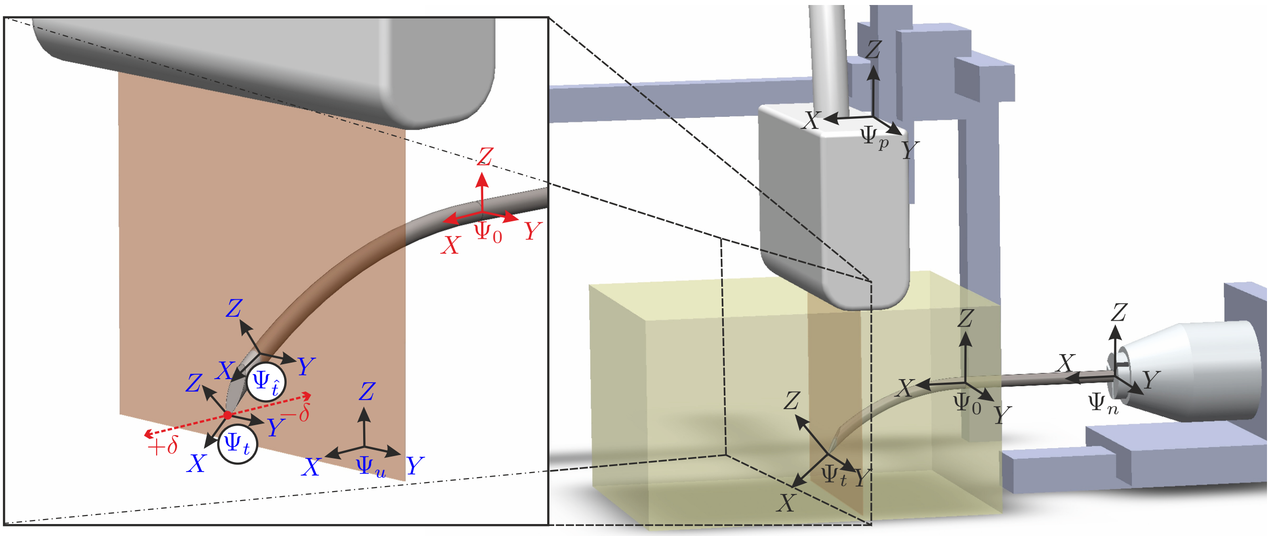

Fig. 3. Overview of the various coordinate systems required to compute the needle tip pose. Frame (Ψ_n) is located at the end-effector of the needle insertion device. Fixed reference frame (Ψ_0) is at the point where the needle enters the soft-tissue simulant, while frame (Ψ_t) is fixed to the needle tip. Frame (Ψ_p) is located at the end-effector of the positioning device, while frame (Ψ_u) is assigned to the two-dimensional ultrasound image. Frame ($\Psi_{\hat{t}}$) is at the needle tip as determined by the controller. The aberration in the transducer along the needle insertion direction is denoted by $\pm\delta$.

must be computed. Positioning the transducer at the needle tip allows the tip frame to be expressed in fixed reference frame by a series of coordinate transformations. Whereby the needle centroid (y_c, z_c), obtained by image processing, describes the needle tip frame with respect to ultrasound image frame. For computational simplicity we assume frames (Ψ_u and Ψ_p) to coincide. The end-effector frame of the positioning device can be expressed in the fixed reference frame by position feedback. The consecutive transformations allow the needle tip position ($\mathbf{p}_t^0$) to be computed. In order to compute ($\mathbf{p}_t^0$) during needle insertion, repositioning of the ultrasound transducer to compensate for out-of-plane motion is required. We assume that needle buckling does not occur during insertion. Thus, the needle tip velocity ($\|\dot{\mathbf{p}}_t^0\|$) equals to the insertion velocity ($\|\mathbf{v}_i\|$),

$$\|\mathbf{v}_i\| = \sqrt{\dot{p}_x^2 + \dot{p}_y^2 + \dot{p}_z^2}. \tag{2}$$

Hence, the needle tip velocity along the x-axis (frame (Ψ_0)) which must be compensated for is given by,

$$\dot{p}_x = \sqrt{\|\mathbf{v}_i\|^2 - \dot{p}_y^2 - \dot{p}_z^2}, \tag{3}$$

where $\dot{p}_y$ and $\dot{p}_z$ are the needle tip deflection velocities calculated by taking time derivatives of needle tip positions (p_y and p_z), respectively. The complete needle tip pose requires orientations (ψ, θ and ϕ) of the needle tip about the x-, y- and z-axes, respectively. Needle tip orientation can not be obtained by direct measurement. Although needle tip rotation about the y- and z-axes can be computed by,

$$\phi = \tan^{-1}\left(\frac{\Delta p_y}{\Delta p_x}\right) \text{ and } \theta = \tan^{-1}\left(\frac{\Delta p_z}{\Delta p_x}\right), \tag{4}$$

respectively. Needle tip orientation about the x-axis (ψ) is obtained from the NID, where we assumed no torsion along the needle shaft during rotation. The orientations (ψ, θ and ϕ) of the needle tip are used to determine rotation matrix ($\mathbf{R}_t^0$). Thus, if the pose is known, the homogeneous transformation ($\mathbf{H}$) can be computed,

$$\mathbf{H}_t^0 = \begin{bmatrix} \mathbf{R}_t^0 & \mathbf{p}_t^0 \\ \mathbf{0}_3^T & 1 \end{bmatrix}, \tag{5}$$

that relates the needle tip frame (Ψ_t) to fixed reference frame (Ψ_0). It is essential to control the transducer to accurately obtain the needle tip pose during insertion.

C. Ultrasound Image-Guided Controller

The controller is used to position the ultrasound transducer, and to obtain position feedback of the needle tip (Fig. 4). The needle tip position is denoted by $\mathbf{p}$, where the velocity ($\dot{\mathbf{p}}$) is calculated by taking the time derivative. For notational simplicity, we do not include frame Ψ_0 in the variables presented in this sub-section. The compensator is used to move the ultrasound transducer according the needle tip velocity ($\dot{p}_x$). Error in the estimation of $\dot{p}_x$ results in a positioning error of the ultrasound transducer along the x-axis (frame (Ψ_0)),

$$\delta = \mid p_x - \hat{p}_x \mid, \tag{6}$$

where $\hat{p}_x$ is the needle tip along x-axis as determined by the controller and δ is the error in transducer position along the x-axis. The needle tip pose error ($\mathbf{E} \in \mathbb{R}^{4\times 4}$) between frames ($\Psi_t$ and $\Psi_{\hat{t}}$) is introduced by δ. Closed-loop control reduces δ. From ultrasound images it can be determined whether the needle is in- or out-of-plane. In the latter case, the ultrasound transducer is positioned ahead of the needle. Thus, by gain scheduling of velocity gain K_e used to move the transducer along x-axis (frame (Ψ_0)), which is

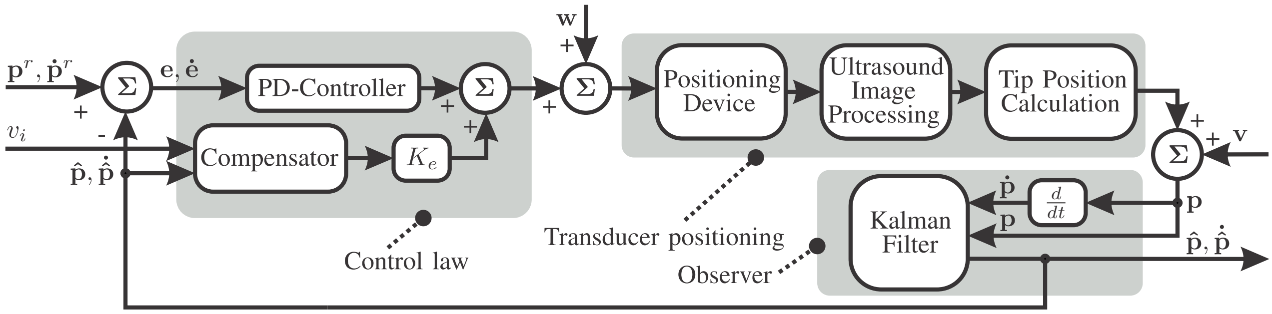

Fig. 4. The controller architecture used to track the needle tip in real-time, as it is inserted through the soft-tissue simulant. Transducer positioning along the x-axis (Ψ_0) is performed by a compensator and gain scheduler (K_e) according (3) and (7), respectively. The proportional-derivative-(PD)-controller (proportional gain ($K_p = 0.4$) and derivative gain ($K_d = 0.1$)) is used to compensate the needle tip motion along the y-axis (frame (Ψ_0)), while motion in z-axis (frame (Ψ_0)) is not compensated for. A cartesian robotic system is used to position the ultrasound transducer at the needle tip to measure its position, which is denoted by $\mathbf{p}$. The time derivative of $\mathbf{p}$ results in $\dot{\mathbf{p}}$. The reference positions and velocities are denoted by $\mathbf{p}^r$ and $\dot{\mathbf{p}}^r$, respectively. The Kalman observer is used to minimize the effects of process ($\mathbf{w}$) and measurement ($\mathbf{v}$) noise on the states ($\mathbf{p}$ and $\dot{\mathbf{p}}$), and to predict the subsequent state.

increased or decreased when the needle is in- or out-of-plane, respectively. Gain scheduling is chosen as,

$$K_e = \begin{cases} 1.05 & \text{if needle is in-plane} \\ 0.5 & \text{if needle is out-of-plane} \end{cases} \tag{7}$$

By employing gain scheduling, the transducer is forced to move towards the needle tip and thus, minimizes δ. In-plane control of the ultrasound transducer along the y-axis (frame Ψ_0) is done by a standard proportional-derivative-(PD)-controller, which allows the needle to move beyond the width (5.5 cm) of the ultrasound transducer. The z-axis (frame Ψ_0) is not controlled during needle tracking, but is used to position the ultrasound transducer at the surface of the soft-tissue simulant. A Kalman observer is added to minimize the influence of noise on the states ($\mathbf{p}$ and $\dot{\mathbf{p}}$), and to predict the subsequent states based on the needle tip velocity [23]. If the ultrasound transducer is placed ahead of the needle, the subsequent states are based on constant needle tip velocity. Without measurement updates the uncertainty of the projected states increase, which makes it important to minimize the duration of measurement absence. The Kalman gain will be adjusted according the increased uncertainty of the predicted states when measurement is available, which ensures a quick decrease in estimation error.

III. Experiments and Validation

This section describes the experimental setup used to track a needle inserted through the soft-tissue simulant. Two types of experiments are performed to evaluate the performance of the needle tip tracking system, and results are presented.

A. Experimental Setup

The experimental setup used to track flexible needles during insertion is shown in Fig. 5. The used needles are fabricated from Nitinol (nickel and titanium alloy, with a Young's Modulus of 75 GPa), which are bevel-tipped with an angle of 30°. Two different needle diameters are used, ϕ 0.5 mm and ϕ 1.0 mm. A gelatin mixture is used to simulate breast-tissue elasticity properties [24]. The elasticity properties of 35 kPa are obtained by mixing (by-weight) gelatin powder (14.9%) (Dr. Oetker, Ede, The Netherlands) with water (84.1%) and silica gel 63 (1.0%) (E. Merck, Darmstadt, Germany) [25]. A realistic testing scenario is provided by adding silica gel, which mimics the acoustic scattering effects in tissue visible in ultrasound images. The needle is inserted by the two-DOF NID. The NID allows the needle to be translated along and rotated about the longitudinal axis [26]. The ultrasound images are obtained by an 18 MHz transducer using a Siemens Acuson S2000 ultrasound system (Siemens AG, Erlangen, Germany). During image acquisition the following settings were used: A frequency of 16 MHz, -12 dB power level and 3 cm scan depth. The images are transferred for image processing to a computer (64-bit, 2.27 GHz Intel Xeon, 12-GB internal memory, 64-bit Windows 7) via S-video output at 25 Hz. The resolution corresponding to the scan depth (3 cm) is 0.12 mm per pixel. The ultrasound transducer is clamped in a three-DOF Cartesian positioning device. The device consists of three orthogonally-placed translational stages LX30, LX26 and LX20 (Misumi Group Inc., Tokyo, Japan) to enable movement in x-, y- and z-axes of frame (Ψ_p) in Fig. 3, respectively. Each stage is actuated by an ECMax22 motor with a GP32/22 gearhead (Maxon Motor, Sachseln, Switzerland), which is velocity controlled by an Elmo Whistle 2.5/60 motor controller (Elmo Motion Control Ltd, Petach-Tikva, Israel). The positioning accuracy of the device is determined at 27 μm, 35 μm and 41 μm along the x-, y- and z-axes (frame (Ψ_p)), respectively. The ultrasound transducer is securely clamped by a 3D-printed holder.

B. Experimental Plan

A reference measurement is used to validate the needle tip pose obtained using ultrasound tracking. The needle tip pose for an undeflected needle can be computed by,

$$\mathbf{H}_t^0 = \mathbf{H}_n^0 \mathbf{H}_t^n, \tag{8}$$

where $\mathbf{H}_n^0$ is the homogeneous transformation from frame (Ψ_n) relative to frame (Ψ_0), and $\mathbf{H}_t^n$ is the transformation matrix from frame (Ψ_t) relative to frame (Ψ_n) (Fig. 3). For an undeflected needle, the homogeneous transformation

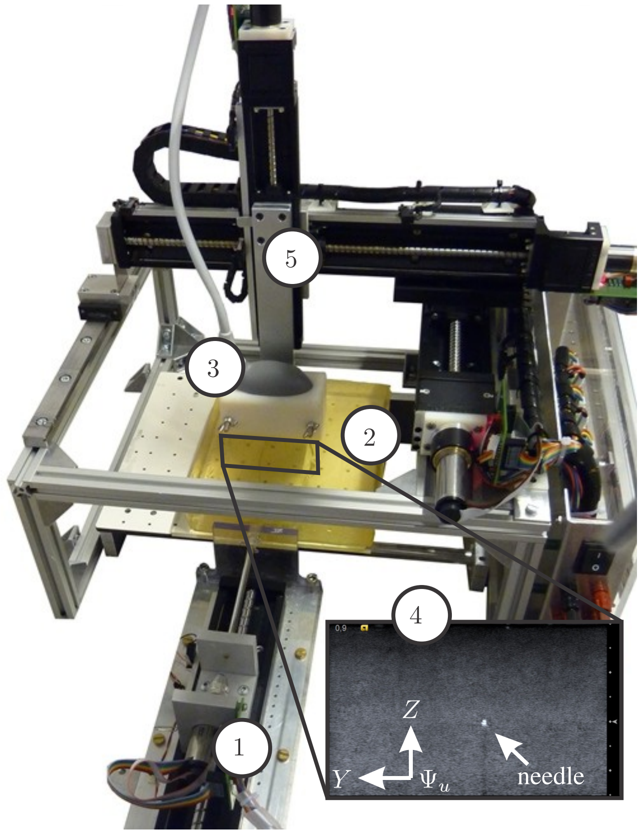

Fig. 5. The experimental setup used for three-dimensional needle tip tracking. ① Needle insertion device. ② Soft-tissue simulant based on gelatin mixture. ③ Ultrasound transducer. ④ Ultrasound image with a radial cross-sectional view of the needle. ⑤ Robotic ultrasound transducer positioning device.

matrix ($\mathbf{H}_t^n$) can be described by a translation mapping in the x-axis (frame (Ψ_0)) equal to the length of the needle. If the needle is rotated during insertion with sufficiently high rotational velocity relative to its insertion velocity, a straight insertion will be achieved i.e., drilling motion (Case I). For such a needle motion profile, the tip pose error between frames ((Ψ_t) and ($\Psi_{\hat{t}}$)) can be formulated by a closed kinematic chain,

$$\mathbf{E} = \mathbf{H}_t^0 \mathbf{H}_n^t \mathbf{H}_0^n, \tag{9}$$

where $\mathbf{E} \in \mathbb{R}^{4\times4}$ represents the needle tip pose error, which is ideally described by the identity matrix. The experiments performed to validate real-time needle tip tracking by evaluating the needle tip pose error ($\mathbf{E}$) are given in Case I (Table I). The accuracy in needle deflection is validated by Case II (Table I). In Case II, the needle is inserted and rotated (360°) over the insertion depth, which results in a helical needle shape. A sweep is performed with a velocity of 3 mm/s to acquire the needle shape. For points along the x-axis (frame (Ψ_0)), the needle deflection in and about y- and z-axes (frame (Ψ_0)) are evaluated. It is assumed that the obtained needle shape remains unchanged after insertion, which allows the static shape data to be compared with real-time needle tip tracking data.

TABLE I

EXPERIMENTAL CASES: CASE I-VALIDATION OF REAL-TIME NEEDLE TIP TRACKING. POSITIONS AND ORIENTATIONS OF THE NEEDLE TIP ARE EVALUATED BY THE NEEDLE TIP POSE ERROR ($\mathbf{E}$). TRACKING IS VALIDATED FOR THREE INSERTION VELOCITIES ($\|\mathbf{v}_i\|$) AND TWO INSERTION DEPTHS (d). A NEEDLE DIAMETER OF ϕ 1.0 MM IS USED. FOR EVERY MILLIMETER INSERTED, A FULL ROTATION (360°) IS PERFORMED. CASE II-VALIDATION OF NEEDLE TIP DEFLECTION DURING INSERTION. THE NEEDLE WITH A DIAMETER OF ϕ 0.5 MM IS INSERTED AND ROTATED (360°) OVER THE INSERTION DEPTH (d) TO OBTAIN A HELICAL SHAPE.

	$\|\mathbf{v}_i\|$ [mm]			d [mm]		
Case	1	3	5	40	80	110
I.1	√			√		
I.2		√		√		
I.3			√	√		
I.4	√				√	
I.5		√			√	
I.6			√		√	
II		√				√

C. Experimental Results

The results from experiments in Cases I and II are provided in Table II. Each experiment is repeated ten times. The mean absolute errors in the tracked tip positions (ϵ_x, ϵ_y and ϵ_z) and orientations ($\epsilon_\theta$and ϵ_ψ) during insertion between frames (Ψ_t and $\Psi_{\hat{t}}$) are reported. In Case I, a ϕ 1.0 mm needle is used to increase the likelihood of a straight insertion. For Case II, a ϕ 0.5 mm needle is used to increase deflection during insertion. Maximum errors in positions are 0.64 mm (Case I.3), 0.25 mm (Case II) and 0.27 mm (Case II) along the x-, y- and z-axes, respectively. Maximum errors in orientation about the y-axis (θ) and z-axis (ϕ) are 2.68° (Case I.4) and 2.83° (Case I.4), respectively.

D. Discussion

In Case I (drilling motion), frame (Ψ_t) is attached to the needle tip which rotates about its x-axis at high rotational velocity (1-5 rotations per second). This results in a continuously interchanging y- and z-axes. Hence, we observe similar values for ϵ_y and ϵ_z. Experiments from Case I show that an increase in needle insertion velocity increases the error (ϵ_x), which could be explained by an increase in aberration of the ultrasound transducer during insertions at higher velocities. By decreasing the needle insertion velocity to 1 mm/s, the maximum error (ϵ_x) is reduced by 166.7%. Further from Case I, it can be observed that for longer insertions (80 mm), the maximum errors (ϵ_y and ϵ_z) both increase by 57.1%. Since different needle insertion velocities show no affect on the needle deflection errors (ϵ_y and ϵ_z) for Case I, Case II is only conducted at 3 mm/s insertion velocity. Although it can not be ruled out that tracking accuracy deteriorates over the insertion depth. In Case II, errors (ϵ_y and ϵ_z) increased by 13.6% and 22.7% as compared to Case I.6, respectively. This could be explained by the increased insertion depth.

IV. CONCLUSIONS AND FUTURE WORK

This study presents a 3D needle tip tracking system that uses 2D ultrasound images. A 2D ultrasound transducer is

TABLE II

NEEDLE POSITION AND ORIENTATION ERRORS FOR CASES I AND II ARE PRESENTED. MEAN ABSOLUTE ERRORS BETWEEN FRAMES (Ψ_t AND $\Psi_{\hat{t}}$) ARE REPORTED WITH THEIR STANDARD DEVIATIONS. ERRORS (ϵ_x, ϵ_y AND ϵ_z) REPRESENTS THE POSITION ERRORS ALONG THE x-, y- AND z-AXES, RESPECTIVELY, WHILE ϵ_θ AND ϵ_ϕ REPRESENT THE ORIENTATION ERRORS ABOUT THE y- AND z-AXES, RESPECTIVELY. *Please refer to the attached video that demonstrates the results of real-time three-dimensional tracking.*

Case	ϵ_x [mm]	ϵ_y [mm]	ϵ_z [mm]	ϵ_θ [degree]	ϵ_ϕ [degree]
I.1	0.24±0.16	0.14±0.04	0.14±0.04	2.57±0.47	2.59±0.47
I.2	0.36±0.10	0.11±0.04	0.11±0.04	1.58±0.32	1.57±0.34
I.3	0.64±0.11	0.13±0.08	0.13±0.10	1.68±0.65	1.69±0.78
I.4	0.24±0.10	0.18±0.08	0.18±0.08	2.68±1.22	2.83±1.36
I.5	0.31±0.01	0.15±0.06	0.15±0.06	1.13±1.32	1.40±1.43
I.6	0.48±0.09	0.22±0.12	0.22±0.12	1.14±0.29	1.19±0.32
II	-	0.25±0.06	0.27±0.06	1.63±0.57	1.39±0.24

placed perpendicular to the needle tip to measure its position in real-time. During insertion a positioning device is used to reposition the ultrasound transducer, which provides needle tip pose feedback. Experiments show maximum errors in tip positions along the x-, y- and z-axes are 0.64 mm, 0.25 mm and 0.27 mm, respectively. Maximum error in tip orientations about y-(θ) and z-(ϕ)-axes are observed as $2.68°$ and $2.83°$, respectively.

For future work, we will combine tracking with needle steering updated by a path planner, which will enable the needle to be steered around an obstacle towards a target. By combining these systems, improved accuracy of minimally invasive medical procedures can be achieved. Also modifications to the ultrasound transducer positioning device will be made to track curved soft-tissue surfaces. Further, the use of needle tip tracking in biological tissue will be investigated.

REFERENCES

[1] J. H. Youk, E.-K. Kim, M. J. Kim, J. Y. Lee, and K. K. Oh, "Missed breast cancers at us-guided core needle biopsy: How to reduce them," *Radiographics*, vol. 27, no. 1, pp. 79–94, 2007.

[2] S. Nag, W. Bice, K. DeWyngaert, B. Prestidge, R. Stock, and Y. Yu, "The american brachytherapy society recommendations for permanent prostate brachytherapy postimplant dosimetric analysis," *International Journal of Radiation Oncology Biology Physics*, vol. 46, no. 1, pp. 221–230, 2000.

[3] H. Fred, "Drawbacks and limitations of computed tomography: views from a medical educator," *Texas Heart Institute Journal*, vol. 31, no. 4, pp. 345–348, 2004.

[4] G. Fischer, I. Iordachita, C. Csoma, J. Tokuda, S. DiMaio, C. Tempany, N. Hata, and G. Fichtinger, "Mri-compatible pneumatic robot for transperineal prostate needle placement," *IEEE/ASME Transactions on Mechatronics*, vol. 13, no. 3, pp. 295–305, 2008.

[5] S. G. Shulman and D. E. March, "Ultrasound-guided breast interventions: Accuracy of biopsy techniques and applications in patient management," *Seminars in Ultrasound, CT, and MRI*, vol. 27, no. 4, pp. 298–307, 2006.

[6] Y.-C. Wu, D.-R. Chen, and S.-J. Kuo, "Personal experience of ultrasound-guided 14-gauge core biopsy of breast tumor," *European Journal of Surgical Oncology (EJSO)*, vol. 32, no. 7, pp. 715–718, 2006.

[7] N. Abolhassani, R. Patel, and M. Moallem, "Needle insertion into soft tissue: A survey," *Medical Engineering and Physics*, vol. 29, no. 4, pp. 413–431, 2007.

[8] J. op den Buijs, M. Abayazid, C. L. de Korte, and S. Misra, "Target motion predictions for pre-operative planning during needle-based interventions," in *Proceedings of the IEEE International Conference on Engineering in Medicine and Biology Society (EMBC)*, pp. 5380–5385, Boston, USA, August 2011.

[9] M. Abayazid, J. Buijs, op den, C. Korte, de, and S. Misra, "Effect of skin thickness on target motion during needle insertion into soft-tissue phantoms," in *Proceedings of the IEEE RAS/EMBS International Conference on Biomedical Robotics and Biomechatronics (BioRob)*, pp. 755–760, Rome, Italy, June 2012.

[10] J. Hong, T. Dohi, M. Hashizume, K. Konishi, and N. Hata, "An ultrasound-driven needle-insertion robot for percutaneous cholecystostomy," *Physics in Medicine and Biology*, vol. 49, no. 3, pp. 441–455, 2004.

[11] V. Kallem and N. Cowan, "Image guidance of flexible tip-steerable needles," *IEEE Transactions on Robotics*, vol. 25, no. 1, pp. 191–196, 2009.

[12] Z. Neubach and M. Shoham, "Ultrasound-guided robot for flexible needle steering," *IEEE Transactions on Biomedical Engineering*, vol. 57, no. 4, pp. 799–805, 2010.

[13] D. Glozman and M. Shoham, "Image-guided robotic flexible needle steering," *IEEE Transactions on Robotics*, vol. 23, no. 3, pp. 459–467, 2007.

[14] R.J. Webster III, J. Memisevic, and A.M. Okamura, "Design considerations for robotic needle steering," in *Proceedings of the IEEE International Conference on Robotics and Automation (ICRA)*, pp. 3588–3594, Barcelona, Spain, April 2005.

[15] J. Engh, G. Podnar, S. Khoo, and C. Riviere, "Flexible needle steering system for percutaneous access to deep zones of the brain," in *Proceedings of the IEEE 32nd Annual Northeast Bioengineering Conference*, pp. 103–104, Easton, USA, April 2006.

[16] H. Neshat and R. Patel, "Real-time parametric curved needle segmentation in 3d ultrasound images," in *Proceedings of the IEEE RAS EMBS International Conference on Biomedical Robotics and Biomechatronics (BioRob)*, pp. 670–675, Scottsdale, USA, October 2008.

[17] P. M. Novotny, J. A. Stoll, N. V. Vasilyev, P. J. del Nido, P. E. Dupont, T. E. Zickler, and R. D. Howe, "Gpu based real-time instrument tracking with three-dimensional ultrasound," *Medical Image Analysis*, vol. 11, no. 5, pp. 458–464, 2007.

[18] J. Stoll, H. Ren, and P. Dupont, "Passive markers for tracking surgical instruments in real-time 3d ultrasound imaging," *IEEE Transactions on Medical Imaging*, vol. 31, no. 3, pp. 563–575, 2012.

[19] M. Aboofazeli, P. Abolmaesumi, P. Mousavi, and G. Fichtinger, "A new scheme for curved needle segmentation in three-dimensional ultrasound images," in *Proceedings of the IEEE International Symposium on Biomedical Imaging: From Nano to Macro (ISBI)*, pp. 1067–1070, Piscataway, USA, July 2009.

[20] C. Nadeau and A. Krupa, "Intensity-based direct visual servoing of an ultrasound probe," in *Proceedings of the IEEE International Conference on Robotics and Automation (ICRA)*, pp. 5677–5682, Shanghai, China, May 2011.

[21] J. E. Aldrich, "Basic physics of ultrasound imaging," *Critical Care Medicine*, vol. 35, no. 5, pp. S131–S137, 2007.

[22] J. Huang, J. Triedman, N. Vasilyev, Y. Suematsu, R. Cleveland, and P. Dupont, "Imaging artifacts of medical instruments in ultrasound-guided interventions," *Journal of Ultrasound in Medicine*, vol. 26, no. 10, pp. 1303–1322, 2007.

[23] Y. Bar-Shalom, X. R. Li, and T. Kirubarajan, *Estimation with Applications to Tracking and Navigation*. New York, USA: John Wiley & Sons., 2001.

[24] A. Gefen and B. Dilmoney, "Mechanics of the normal woman's breast," *Technology and Health Care*, vol. 15, no. 4, pp. 259–271, 2007.

[25] R. Roesthuis, M. Abayazid, and S. Misra, "Mechanics-based model for predicting in-plane needle deflection with multiple bends," in *Proceedings of the IEEE RAS/EMBS International Conference on Biomedical Robotics and Biomechatronics (BioRob)*, pp. 69–74, Rome, Italy, June 2012.

[26] R. J. Roesthuis, Y. R. J. van Veen, A. Jahya, and S. Misra, "Mechanics of needle-tissue interaction," in *Proceedings of the IEEE/RSJ International Conference on Intelligent Robots and Systems (IROS)*, pp. 2557–2563, San Francisco, USA, September 2011.

Part III

‘Three-Dimensional Needle Path Planning and Steering using Two-Dimensional Ultrasound Images’

Three-Dimensional Needle Path Planning and Steering using Two-Dimensional Ultrasound Images

Gustaaf J. Vrooijink[*1], Momen Abayazid[*], Sachin Patil[†], Ron Alterovitz[†] and Sarthak Misra[*]
[*] MIRA-Institute for Biomedical Technology and Technical Medicine, University of Twente, The Netherlands
[†] Department of Computer Science, University of North Carolina at Chapel Hill, USA

Abstract

Needle insertion procedures are commonly used in minimally invasive surgery (MIS). In this paper, we develop a three-dimensional closed-loop control algorithm to robotically steer flexible needles with an asymmetric tip towards a target in a soft-tissue simulant. A novel technique which uses two-dimensional ultrasound is used to track the needle tip motion and provides the needle tip pose. The needle tip pose is used in a customized rapidly exploring random trees based motion planner to determine the needle trajectory. The needle is steered in an environment where obstacle and target motion occur. In order to evaluate the proposed needle steering method, experiments are performed which show targeting errors of 3.45 mm (RMS).

1. Introduction

Needle insertion into soft tissue is a common minimally invasive surgical procedure. Percutaneous needles are used for diagnostic and therapeutic purposes such as biopsy and brachytherapy, respectively. Imaging modalities such as ultrasound and magnetic resonance (MR) images, and computed tomography (CT) scans are often used during needle insertion procedures to determine the positions of the needle and target for accurate needle tip placement. Inaccurate placement may result in misdiagnosis during biopsy, and unsuccessful treatment during brachytherapy. Rigid needles are used in such procedures, but they do not provide the clinician with sufficient

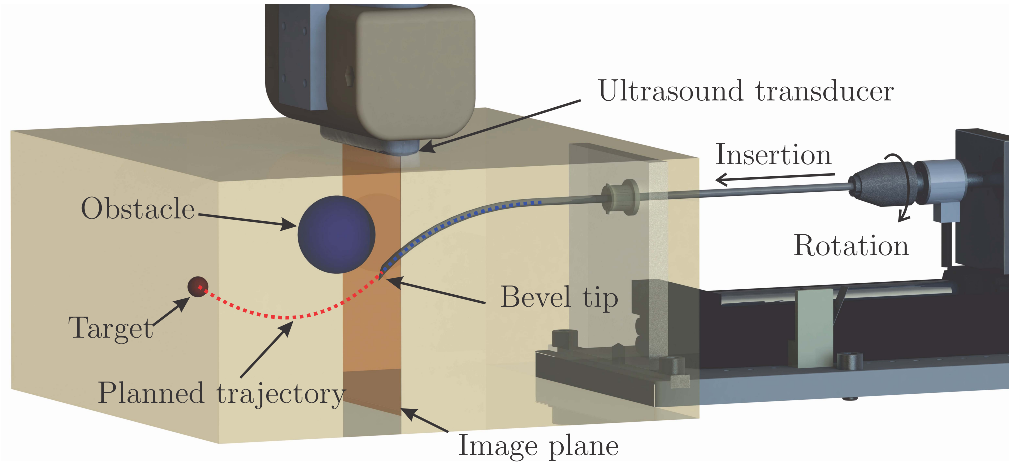

Figure 1: A flexible bevel-tipped needle is steered in the soft-tissue simulant by using a device that inserts and rotates the needle. The needle deflects along a curved trajectory in the direction of the bevel tip. A two-dimensional ultrasound transducer, which is orientated perpendicular to the needle insertion direction, is used to track the needle tip in three-dimensional space during insertion. A transducer positioning device is used to track the needle tip during insertion in order to compute the needle tip pose. The needle tip pose is used to plan and control the needle motion along a desired trajectory to reach a target while avoiding obstacles.

steering capabilities to reach the intended target [2]. Flexible needles were introduced to facilitate curved paths to reach the target. They are used to avoid sensitive tissue that might be located along the needle path [17, 20, 7]. Flexible needles with an asymmetric tip (bevel tip) naturally deflects during insertion into soft tissue [33, 23]. Needle deflections due to tip-asymmetry is used to steer the needle towards a target [2, 20].

In recent studies, models for needle deflection were presented. These models are used to steer the flexible needle in two-dimensional (2D) space, as in the clinical setting, needle insertion is guided by medical imaging modalities (ultrasound, CT, and MRI). Thus, many studies focused on 2D motion planning [4, 5, 28]. DiMaio and Salcudean presented a path planning algorithm that relates the needle motion at the base (outside the soft-tissue phantom) to the tip motion inside the tissue [9]. A three-dimensional (3D) deflection model of bevel-tipped flexible needles was developed by Duindam *et al.* [11]. Several studies presented a 3D path planning models based on Rapidly-exploring Random Trees (RRTs) [27, 30, 34]. These studies demonstrated simulation results to verify the models. A steering algorithm is required to validate the models experimentally.

Steering algorithms were developed to control the needle to follow the planned path. Glozman and Shoham developed an image-guided closed-loop control algorithm for steering flexible needles [16]. Fluoroscopic images were used for feedback of the needle position during insertion. The flexible needle was modeled as a beam supported by virtual springs. They solved forward and inverse kinematics of the needle for path planning. Neubach and Shoham used ultrasound scanning for image-guided 2D steering [24]. Hauser *et al.* developed a 3D feedback controller that steers the needle along a helical path [18]. The results of Hauser *et al.* were based on simulations, and experiments were not performed for validation. Experimental validation of the path planning and steering algorithms requires real-time tracking of the needle during insertion.

Needle tracking techniques were developed based on ultrasound and fluoroscopic image segmentation to determine the needle shape during the insertion procedure [16, 24]. The spatial resolution of 3D ultrasound images is limited and the refresh rate of a 3D image in low [25], and the use of x-ray-based imaging (CT or fluoroscopy) exposes the patient to high doses of ionizing radiation [14]. MR imaging suffers from low refresh rate and incompatibility with magnetic materials [10]. Electromagnetic position tracking sensors [2, 15] are used for 3D needle tracking, but its accuracy is sensitive to ferromagnetic materials in the range of measurement.

A novel technique is presented to track flexible needles in 3D using a 2D ultrasound transducer. The 2D ultrasound transducer is placed at the needle tip, perpendicular to the direction of needle insertion (Fig. 1). The transducer is repositioned during insertion at the needle tip by a positioning device, which allows for computation of the tip pose. Repositioning of the transducer enables 3D real-time tracking of the needle tip through the soft-tissue simulant. The needle tip pose is used for path planning to determine feasible needle trajectories to reach a target.

The developed path planning algorithm is used to estimate the needle trajectory during insertion. The algorithm computes feasible needle trajectories during insertion (online), and selects the optimal trajectory using clinically motivated criteria such as minimizing insertion length or maximizing the distance to obstacles. The needle steering method is implemented by using duty cycling spinning of the needle during insertion [13]. Duty cycling relaxes the constraint on constant-curvature of the needle allowing any curvature between straight and the constant radius of curvature. To the best of our knowledge, the use of 3D ultrasound tracking combined with 3D path planning for needle steering to reach a moving target while avoiding an obstacle has not been demonstrated experimentally.

This paper is organized as follows: Section 2.1 explains the methods used for real-time needle tip pose computation. Sections 2.2 and 2.3 describes the methods used for 3D motion planning and flexible needle steering, respectively. Section 2.4 discusses the experimental setup. The experimental plan, results and discussion are provided in Section 3, followed by conclusions and recommendations for future work in Section 4.

2. Methods

This section presents the methods to track, plan and steer flexible needles to avoid an obstacle and reach a target. First, the estimation of the needle tip pose is described. Further, the path planning method used to determine the optimal needle trajectory to reach a target while avoiding obstacles is presented. Subsequently, the needle steering method to control the needle motion is given. Finally, the experimental setup is presented.

2.1. Ultrasound Needle Tip Tracking

The method to track the flexible needle tip in 3D space using 2D ultrasound images is presented in this subsection. First, the processing of ultrasound images to determine the needle location is described. Subsequently, the needle location in ultrasound images is used to compute the needle tip pose. Finally, the controller used to position the ultrasound transducer at the needle tip is explained.

2.1.1. Ultrasound Image Processing

Ultrasound images are processed to compute the needle tip pose which is used for needle steering. The 2D ultrasound transducer is placed perpendicular to the needle insertion axis as shown in Fig. 1. The resulting 2D ultrasound image provides a radial cross-sectional view of the needle. The ideally circular shape of the radial cross-sectional view of the needle is deformed by an artifact known as reverberation (Fig. 2(a)). The artifact occurs when sound waves are repeatedly reflected between materials with acoustic impedance differences [3]. These differences in acoustic impedance between needle and soft-tissue simulant causes multiple bouncing sound waves in the needle before returning back to the transducer. The resulting artifact, which

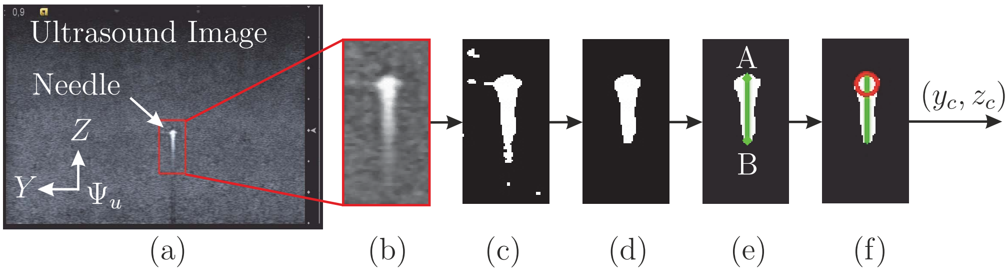

Figure 2: The ultrasound image processing steps performed to determine the needle centroid position (y_c,z_c). (a) The ultrasound image shows a radial cross-sectional view of the needle affected by the comet tail artifact (CTA). A cropped section from this image is used for image processing. (b) A median filter is applied to reduce speckle in the ultrasound image. (c) Thresholding is used to obtain a binary image of the needle. (d) Erosion and subsequently dilation are applied to remove the remaining speckle in the ultrasound image. (e) A feature extraction algorithm (Hough Transform) is used to find a vertical line segment denoted by $\overline{AB}$, which describes the needle with CTA. (f) The needle centroid position (y_c,z_c) is evaluated from A in the direction of B at a distance equal to the needle radius, and displayed as the center of the red circle.

is visible in ultrasound images has a tail-shaped structure of equally spaced echoes along the sound wave. The length of the tail-shaped structure depends on the bouncing echoes that are received by the transducer. The artifact is often referred to as the comet tail artifact (CTA) [19].

An image processing method is developed to locate the needle centroid from the radial cross-sectional view of the needle which is affected by the CTA. The proposed method consists of a series of image processing techniques used to determine the needle centroid independent of the influences of the CTA. The needle in ultrasound images is enhanced by a series of basic image processing techniques, including median filtering, thresholding, and erosion and dilation in Fig. 2(b),(c) and (d), respectively. The enhanced image of the needle is used to determine the needle centroid. A feature extraction algorithm based on Hough transform is used to find a set of vertical line segments which describe the needle centroid affected by the CTA. The length of each line segment must be equal or greater than the needle diameter. A mean line segment ($\overline{AB}$) is determined using the set of vertical line segments (Fig. 2(e)). The line segment ($\overline{AB}$) describes the needle with CTA under the assumption that the tale shaped structure of the CTA is symmetric along the sound wave. Variations in the size of the tail shaped structure are dependent on the echoes that return to the transducer and affect the mean line segment at B. Point A of mean line segment ($\overline{AB}$) is not affected by the CTA, and represents a point on the surface of the needle which is used to determine the needle centroid location. The needle centroid (y_c, z_c) is determined from A in the direction B at a distance equal to the radius of the needle (Fig. 2(f)). The transducer is positioned above the needle tip during insertion to calculate the needle tip position (centroid (y_c, z_c)). This is used to compute the needle tip pose.

2.1.2. Needle Tip Pose Computation

The coordinate frames required to determine the needle tip pose during insertion are shown in Fig. 3. The needle is inserted in the soft-tissue simulant along the x-axis (frame (Ψ_0)) with an insertion velocity $(\mathbf{v}_i)$ using a needle insertion device (NID). The NID also facilitates needle rotation about the x-axis (frame (Ψ_0)), which allows the needle to bend in a controlled direction. In order to determine the needle tip pose as it moves through the soft-tissue simulant, the needle tip position,

$$\mathbf{p}_t^0 = \begin{bmatrix} p_x & p_y & p_z \end{bmatrix}^T, \tag{1}$$

with respect to the fixed reference frame (Ψ_0) is computed. The needle centroid (y_c, z_c), describes the computed tip frame $(\Psi_{\hat{t}})$ in the ultrasound image frame (Ψ_u). The frames (Ψ_u and Ψ_p) coincide for computational simplicity. Frame (Ψ_p) is attached to the positioning device end-effector, and is used to describe the transducer position with respect to frame Ψ_0. Thus, by using coordinate transformations, the needle tip position $(\mathbf{p}_t^0)$ can be expressed in the fixed reference frame. In order to compute $\mathbf{p}_t^0$, the ultrasound image plane must be located at the tip. Therefore, the transducer needs to be repositioned along the insertion axis (x-axis of frame (Ψ_0)) according to the needle tip motion. It is assumed that the needle does not buckle during insertion. Hence, the needle tip velocity $(\|\dot{\mathbf{p}}_t^0\|)$ equals to the insertion velocity $(\|\mathbf{v}_i\|)$ at the base,

$$\|\mathbf{v}_i\| = \sqrt{\dot{p}_x^2 + \dot{p}_y^2 + \dot{p}_z^2}. \tag{2}$$

This relation can be used to determine the required transducer motion along the x-axis (frame (Ψ_0)) to compensate for the needle tip motion. Thus, by rewriting (2), the required transducer motion is given by,

$$\dot{p}_x = \sqrt{\|\mathbf{v}_i\|^2 - \dot{p}_y^2 - \dot{p}_z^2}, \tag{3}$$

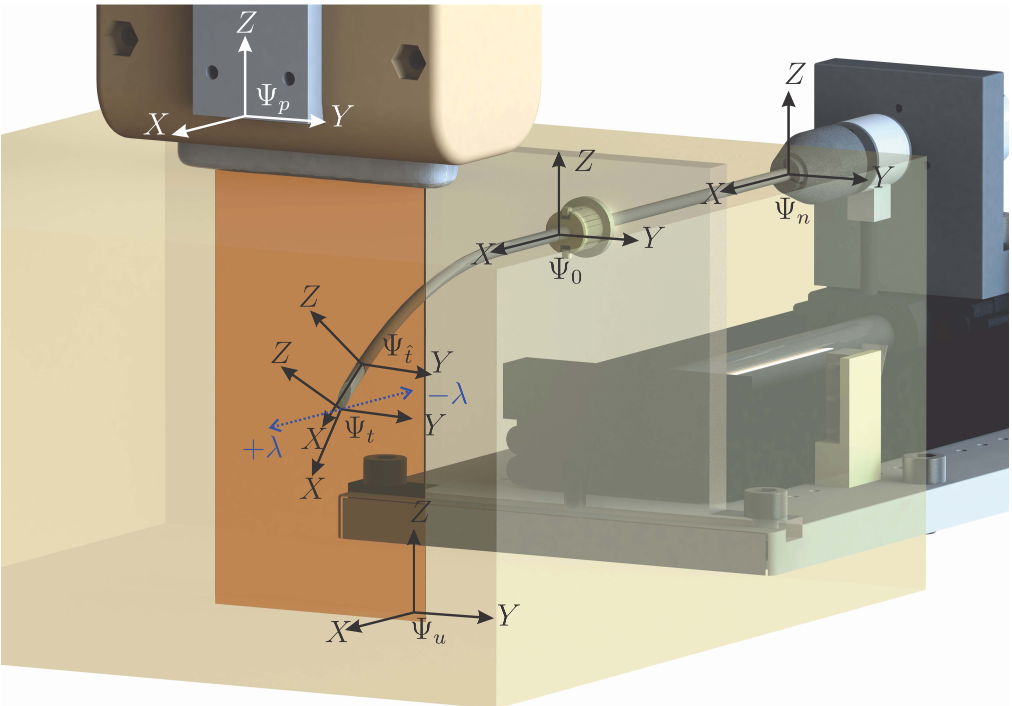

Figure 3: The various coordinate frames used to compute the needle tip pose: Frame (Ψ_0) is used as fixed reference frame located at the needle entry point. Frame (Ψ_n) is attacted to the needle insertion device end-effector, while frame (Ψ_p) is located at the end-effector of the transducer positioning device. Frame (Ψ_u) is fixed to the ultrasound image plane. Frame (Ψ_t) is located at the needle tip, while frame ($\Psi_{\hat{t}}$) is fixed at the computed needle tip location. The ultrasound transducer aberration along the needle insertion axis (x-axis of frame Ψ_0) is denoted by $\pm\lambda$.

where the insertion velocity is corrected using the tip velocities ($\dot{p}_y$ and $\dot{p}_z$) which are the derivatives of needle tip positions (p_y and p_z), respectively. In order to compute the needle tip pose, orientations of ψ, θ and ϕ (about the x-, y- and z-axes, respectively) are required. The NID controls the needle tip orientation about its x-axis. Torsional stiffness of the needle shaft is assumed. Hence, the needle tip orientation about the x-axis can be determined from the NID (frame (Ψ_n)). The orientation of the needle about the y-axis (θ) and z-axis (ϕ) are not directly computed. These tip orientations are computed

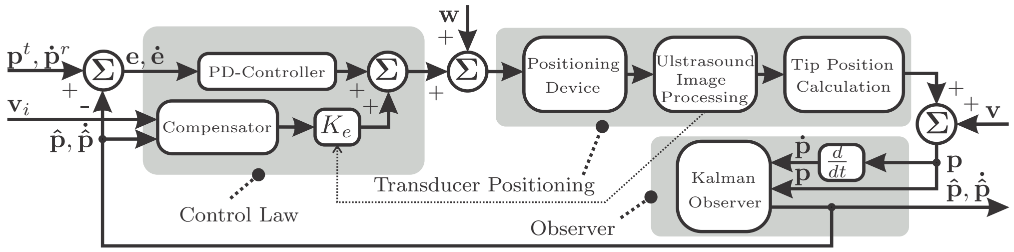

Figure 4: An overview of the controller architecture to control the transducer motion in order to enable real-time three-dimensional needle tip tracking. The transducer motion along the x-axis (frame (Ψ_0)) is computed by the compensator using the needle insertion velocity $\mathbf{v}_i$ according to (3). In order to provide closed loop control, gain scheduling (K_e) according to (8) is applied. In-plane motion (y-axis of frame (Ψ_0)) of the needle tip is compensated by a proportional-derivative-(PD)-controller (proportional gain $(K_p = 0.4)$ and derivative gain $(K_d = 0.1)$). The needle tip motion in the z-axis (frame (Ψ_0)) is not compensated for, instead it is used to keep contact between the transducer and the soft-tissue simulant. The transducer motion is enabled by a Cartesian positioning device and used to provide the needle tip position $(\mathbf{p})$. The needle tip velocity $(\dot{\mathbf{p}})$ is obtained by taking the time derivative of $\mathbf{p}$. The tracker reference signals are denoted $\mathbf{p}^r$ and $\dot{\mathbf{p}}^r$, while the tracker errors are denoted $\mathbf{e}$ and $\dot{\mathbf{e}}$, respectively. The process $(\mathbf{w})$ and measurement $(\mathbf{v})$ noises on the states ($\mathbf{p}$ and $\dot{\mathbf{p}}$) are minimized by a Kalman observer, which also predict the subsequent state. The estimated needle tip position and velocity are denoted $\hat{\mathbf{p}}$ and $\dot{\hat{\mathbf{p}}}$), respectively.

by,

$$\theta = \tan^{-1}\left(\frac{\Delta p_z}{\Delta p_x}\right) \text{ and } \phi = \tan^{-1}\left(\frac{\Delta p_y}{\Delta p_x}\right), \tag{4}$$

respectively. The rotation matrix $(\mathbf{R}_t^0)$ is computed using the tip orientations (ψ, θ and ϕ). The tip pose is known, since position $(\mathbf{p}_t^0)$ and orientation $(\mathbf{R}_t^0)$ are known. Hence, the homogeneous transformation is given by,

$$\mathbf{H}_t^0 = \begin{bmatrix} \mathbf{R}_t^0 & \mathbf{p}_t^0 \\ \mathbf{0}_3^T & 1 \end{bmatrix}, \tag{5}$$

which describes the needle tip frame (Ψ_t) with respect to the reference frame (Ψ_0). In order to calculate the needle tip pose during insertion, a controller is implemented to position the ultrasound transducer accurately.

2.1.3. Ultrasound Image-Guided Controller

The ultrasound transducer is positioned at the needle tip using the controller architecture presented in Fig. 4. The needle tip position is denoted by $\mathbf{p}$, and its corresponding time derivative representing the tip velocity by $\dot{\mathbf{p}}$. Unless otherwise stated, the variables used in this sub-section are expressed in the fixed reference frame (Ψ_0), which is not included in the notation for simplicity. The transducer moves in the needle insertion direction (x-axis of frame (Ψ_0)) using a compensator according to the computed needle tip velocity ($\dot{p}_x$) (3). Improper estimation of velocity ($\dot{p}_x$) results in a positioning error between transducer and needle tip along the x-axis (frame (Ψ_0)), which is considered to be the transducer aberration denoted by λ. The aberration is given by,

$$\lambda = \mid p_x - \hat{p}_x \mid, \tag{6}$$

where p_x represents the needle tip position and $\hat{p}_x$ its estimate provided by the controller. The transducer aberration (λ) introduces an error in the computed needle tip pose,

$$\mathbf{H}_t^{\hat{t}} = \mathbf{H}_0^{\hat{t}}\mathbf{H}_t^0, \tag{7}$$

where $\mathbf{H}_t^{\hat{t}} \in \mathbb{R}^{4\times4}$ represents the pose error between frames (Ψ_t and $\Psi_{\hat{t}}$), which ideally equals the identity matrix.

Closed-loop control is required to minimize the computed needle tip pose error. The computed needle tip pose error is reduced by minimizing the transducer aberration (λ). This is achieved by adding a velocity gain (K_e) to the computed velocity ($\dot{p}_x$), which provides additional control. Thus, by scheduling of K_e, the transducer velocity can be increased or decreased when the needle is in- or out-of-plane, respectively. Hence, by scheduling of the velocity gain according to

$$K_e = \begin{cases} 1.05 & \text{if needle is in-plane} \\ 0.5 & \text{if needle is out-of-plane} \end{cases}, \tag{8}$$

closed loop control is achieved (K_e is estimated empirically). The imposed gain scheduling controller forces the transducer to move towards the needle tip, and thus, minimizes λ. A standard proportional-derivative-(PD)-controller is used to control the transducer motion along the y-axis (frame Ψ_0), and this allows the needle tip to move beyond the transducer image width (5.5 cm). The transducer does not move according to the needle tip position along the z-axis (frame Ψ_0). Transducer motion along the z-axis (frame Ψ_0) is primarily used to maintain contact between the transducer and the soft-tissue simulant surface to provide clear ultrasound images. In order to minimize the influence of process and measurement noise on the states ($\mathbf{p}$ and $\dot{\mathbf{p}}$), a Kalman observer is added [6]. Further, the Kalman observer is used to determine the subsequent states. If the transducer moves ahead of the needle (loss of visibility), the subsequent states are computed using the needle tip velocity. The uncertainty of the projected states over time increases without measurement updates. Hence, it is essential to minimize the duration of measurement absence. Upon return of measurement data, the Kalman gain will be adapted according the increased uncertainty of the projected states, ensuring a decrease in estimation error.

2.2. Motion Planning

We use a fast motion planner for steerable needles presented by Patil et al. in a closed-loop fashion under ultrasound image-guidance to automatically reach targets in 3D environments while avoiding obstacles and compensating for real-world uncertainties [27]. In contrast to the standard practice of planning a feasible trajectory and using a feedback controller for correcting uncertain perturbations, the motion planner is fast enough to correct for perturbations in needle, obstacle, or target motion as they occur. This eliminates the need for a separate feedback controller, which is difficult to create and tune for under-actuated, nonholonomic devices like steerable needles.

The motion planning algorithm is based on a customized, sampling-based rapidly exploring random trees motion planner that speeds up needle steering motion planning to the point that it can be done in real-time with typical needle insertion velocities [21]. Prior work on motion planning for steerable needles in 3D assumes that the curvature is a constant, which severely restricts the range of motion of the needle tip [34, 12, 26]. This makes it difficult for planners to compute a feasible motion plan in 3D environments with obstacles, thus sacrificing optimality or completeness. In contrast, the planner assumes a variable curvature kinematic model that allows us to compute trajectories composed of circular arcs of bounded curvature and uses duty cycled spinning during insertion to adjust the needle's net curvature [22]. The planner also makes use of reachability-guided sampling for efficient expansion of the rapidly-exploring search tree to significantly improve planner performance [30]. These customizations help us achieve orders of magnitude reduction in computation time compared to prior sampling-based planners and make the planner suitable for closed-loop needle steering [34]. We refer the reader to Patil et al. for additional details on the planning algorithm [34].

Given preoperative medical images, the clinician can specify the insertion location and target region as well as sensitive structures such as glands or blood vessels, and other obstacles such as bones. After specifying the entire environment, the planner computes an initial plan. The corresponding computed control outputs are used to predict the needle tip pose after execution of these controls. The computed controls are then applied to the needle, while simultaneously the predicted tip pose is used for replanning. The planner then operates in a closed-loop fashion by constantly replanning using the predicted needle tip pose evaluated from the actual needle tip pose ($\mathbf{H}_t^0$) (5) obtained from the ultrasound tracking system. We also take into account the actual positions of the target and the obstacles at each replanning step. At each step, multiple feasible motion plans are computed and a high quality plan is selected based on clinically motivated criteria such as minimizing the length of the path (to minimize tissue cut) or maximizing clearance from obstacles (to maximize safety). The first set of control inputs comprising of the insertion and twist speeds is sent to the needle insertion device for execution and the process is repeated till the needle reaches the target (see Fig. 5).

2.3. Duty Cycled Needle Steering

The planner computes a sequence of variable curvature circular arcs that steers the needle from the specified needle tip pose to the target. However, the needle is only capable of following constant curvature paths when inserted in soft-tissue simulants. We approximate any curvature (κ) between 0 and the maximum natural curvature (κ_0) by duty cycling the rotation of the needle [22]. The variable curvature (duty cycling) is achieved by alternating between (I) insertion with rotation, in which the needle moves straight by spinning at a constant, and (II) insertion without rotation, in which the needle follows a path of maximum curvature, rate. Needle spinning must be a multiple of full rotations in order to preserve the same axial angle every time. Duty cycling is implemented for needle steering by moving a fixed distance each cycle and spinning with a fixed twist speed (ω_{spin}). Let δ be the duration of each duty cycling interval, which is composed of a spin interval of duration (δ_{spin}) and an insertion interval of duration (δ_{ins}), as illustrated in Fig. 6(a). Let α ($0 \leq \alpha \leq 1$) be the proportion of the time spent in spin intervals, i.e., $\alpha = \delta_{\text{spin}}/\delta$, where $\delta = \delta_{\text{spin}} + \delta_{\text{ins}}$. The empirical relationship

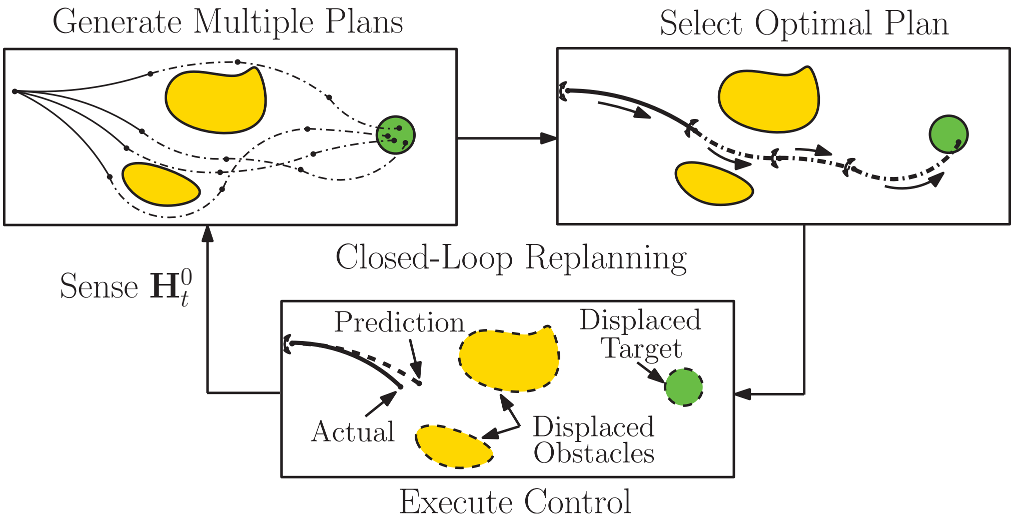

Figure 5: Closed-loop needle steering via fast replanning: Given the actual needle tip pose, target region, a specification of the obstacles in the environment, and characterization of the steerable needle's properties, we use a fast, randomized motion planner to compute in the available time many feasible motion plans (top left). The method selects the best plan based on clinically motivated optimization criteria such as minimizing path length or maximizing clearance from obstacles (top right). We execute the first control input of the plan and measure the needle tip pose using the ultrasound tracking system (bottom). The actual tip pose deviates from the predicted pose because of uncertainty. We repeat the planning process, hence replanning, starting from the actual tip pose. We also provide the displaced target position and displaced configurations of obstacles in the environment as input to the planner. Closed-loop steering is capable of automatically steering the needle to targets in three-dimensional environments while avoiding obstacles and correcting perturbations in needle, obstacle, or target motion as they occur.

between κ and α is expressed as:

$$\alpha = h(\kappa),\ 0 \leq \kappa \leq \kappa_0, \tag{9}$$

where $h(\kappa)$ is dependent on the mechanical properties of the needle and soft-tissue simulant and is determined by fitting a polynomial function to the empirical data gathered during characterization experiments as described below.

Given a circular arc of desired curvature (κ), we use (9) to determine α. Since the needle tip arrives at the same axial angle at the end of each spin interval, the duration of the spin interval $\delta_{\text{spin}} = (2k\pi/\omega_{\text{spin}}), k \in \mathbb{Z}$. We then

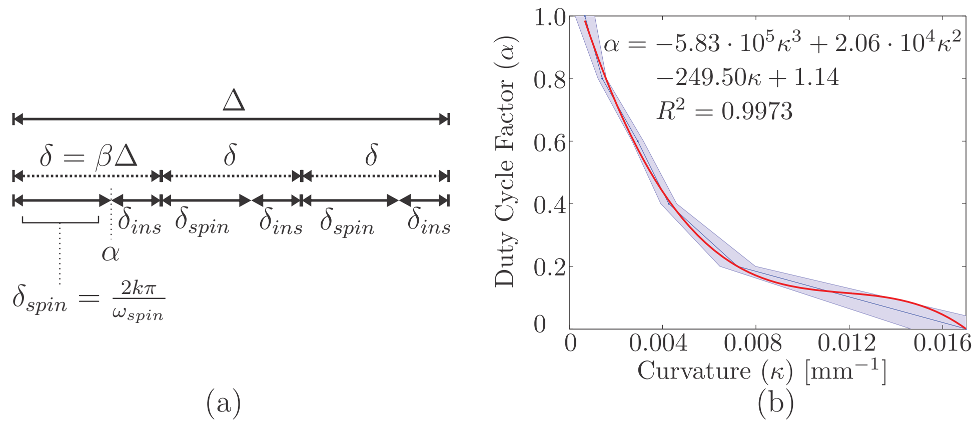

Figure 6: (a) The time duration (Δ) is split into multiple (three) intervals of duration δ each for $\beta = 1/3$. Each interval is then composed of two intervals: (I) a spin interval of duration $\delta_{\text{spin}} = (2k\pi/\omega_{\text{spin}}), k \in \mathbb{Z}$ in which the needle is both inserted and rotated, and (II) an insertion interval of duration δ_{ins} in which the needle is only inserted without any rotation. (b) Characterization of the relationship $\alpha = h(\kappa)$ for needle insertion in the soft-tissue simulant.

compute the quantities $\delta = (\delta_{\text{spin}}/\alpha)$ and $\delta_{\text{ins}} = (\delta - \delta_{\text{spin}})$. The low level control inputs during a duty cycle interval are given by:

$$v(t) = \quad v_{\text{ins}}, \qquad 0 \leq t \leq \Delta/\delta \tag{10}$$

$$\omega(t) = \begin{cases} \omega_{\text{spin}} & \text{if} \quad j\delta < t \leq j\delta + \delta_{\text{spin}} \\ 0 & \text{if} \quad j\delta + \delta_{\text{spin}} < t \leq (j+1)\delta \end{cases}, \tag{11}$$

where v_{ins} is the default insertion speed of the needle, $j \in \{0, 1, \ldots, \Delta/\delta\}$, and Δ/δ is the total number of duty cycle intervals required to span the duration of each replanning step Δ. This allows us to compute the control inputs required for actuation (insertion and twists) of the needle.

Duty cycling requires that we characterize the maximum curvature (κ_0) of the needle and determine the empirical relationship ($h(\kappa)$) between the curvature (κ) and the duty cycling factor (α). We empirically determined that $h(\kappa)$ is dependent on the mechanical properties of the needle and the tissue and is not necessarily linear as demonstrated by prior work with duty cycled needle steering [22]. To construct the relationship ($h(\kappa)$), we varied the value of α between 0 and 1 in increments of 0.2. We then computed the duration of the duty cycling interval (δ) for a time interval $\Delta = 1.66$ sec.

Given a fixed insertion speed (v_{ins}) and twist speed (ω_{spin}), we command the actuators during each duty cycling interval with control inputs computed using (11).

The application of these controls causes the needle tip to traverse a circular arc of variable curvature κ in a plane. We performed repeated insertions of the needle for up to 50 mm in the soft-tissue simulant. We computed a best-fit polynomial curve with a fixed maximum degree (= 3) that minimized the sum of the squared errors of the data points from the curve. This curve defines the relationship $\alpha = h(\kappa)$. An important point to note is that the smaller the distance ($v_{\text{ins}}\delta$) traveled by the needle tip in every duty cycling interval, the better the approximation of κ. We used an insertion distance of 5 mm per duty cycling interval for our experiments.

To determine the effective curvature (κ) of the planar arc, we recorded the needle tip pose ($\mathbf{H}_t^0$) after the end of each duty cycling interval for N such intervals. We observed that the needle tip deviated from the plane because of initialization errors and other sources of uncertainty. To robustly estimate κ, we fit a circle to the set of 3D points given by $\mathbf{p}_t^0 \in \mathbb{R}^3, t = 0, \ldots, N$. We accomplished this by first computing a best-fit plane that minimized the sum of the squared orthogonal distances from each point to the plane by performing principal component analysis (PCA) on the set of points. We then projected the points onto the first two principal components that span the plane and then fitted a circle to the set of projected 2D points using a robust circle fitting algorithm [31]. The curvature (κ) was obtained by taking the reciprocal of the radius of this fitted circle. Fig. 6(b) shows the relationship $\alpha = h(\kappa)$ for needle insertion in soft-tissue simulant used for our experiments. The needle achieved a maximum curvature $\kappa_0 = 0.017\,$,mm^{-1}.

2.4. Setup

The experimental setup which is dispayed in Fig. 7 can be divided into two parts. First, the insertion device in which the needle is allowed to be inserted and rotated about its axis. A telescopic sheath surrounds the needle to prevent buckling during insertion into the soft-tissue phantom. The details of the needle insertion device are presented in [32, 29]. The setup also includes a transducer positioning device which allows the ultrasound transducer to move in 3D. The transducer positioning device consists of three linear translation stages LX30, LX26 and LX20 (Misumi Group Inc., Tokyo, Japan) to enable movement in x-, y- and z-axes (frame (Ψ_0)) (Fig. 3), respectively. An ECMax22 motor with a GP32/22 gearhead (Maxon Motor,

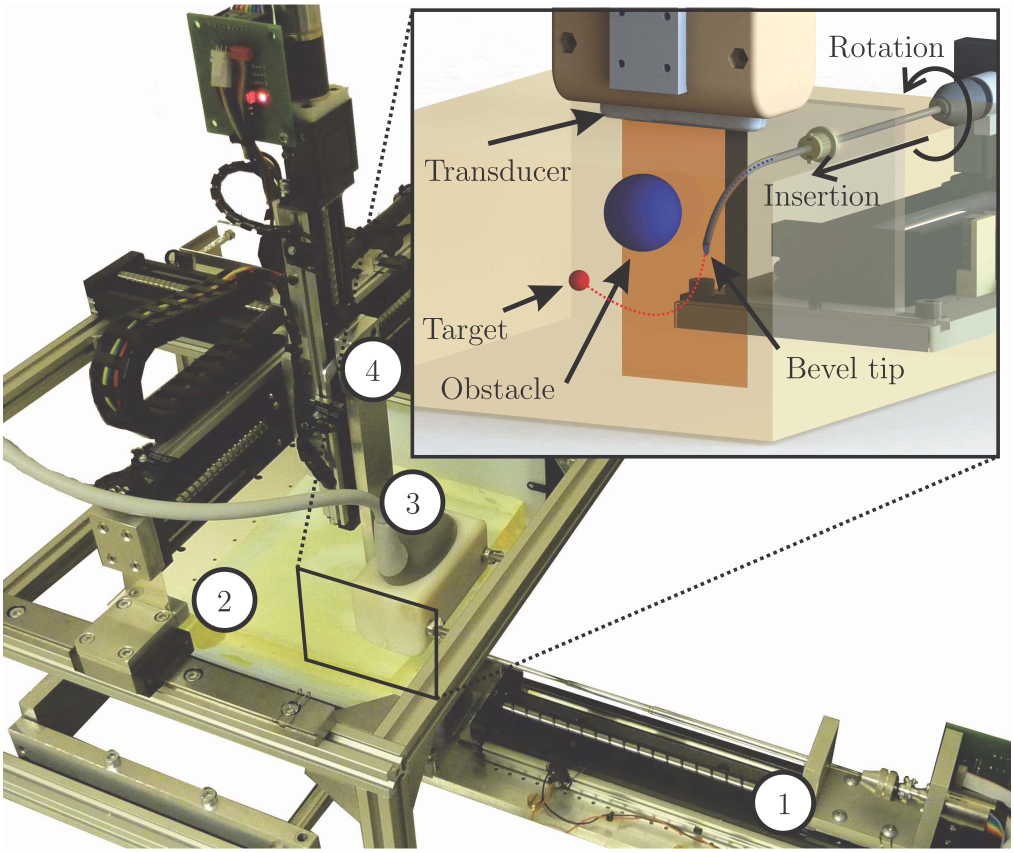

Figure 7: The experimental setup used to track and steer a flexible needle to reach a target while avoiding an obstacle. The needle, which is controlled at its base (inset) by a needle insertion device ① is inserted into the soft-tissue simulant ②. The two-dimensional ultrasound transducer ③ is positioned above the needle tip during insertion by a transducer positioning device ④, which provides feedback for steering.

Sachseln, Switzerland), is used to actuate the linear stages. The velocity of each stage is controlled by an Elmo Whistle 2.5/60 motor controller (Elmo Motion Control Ltd, Petach-Tikva, Israel). The positioning accuracy of the device is 27μm, 35μm and 41μm along the x-, y- and z-axes, respectively. A clamp is used to attach the ultrasound transducer to the linear stages of the positioning device. The ultrasound images are obtained using an 18 MHz transducer connected to a Siemens Acuson S2000 ultrasound machine (Siemens AG, Erlangen, Germany). The ultrasound machine is linked to a computer using an S-video cable that transfers the images (720×576 pixels) with a frame rate of 25 frames per second.

The ultrasound images are used to track the needle during insertion into a soft-tissue simulant. The soft-tissue simulant is made of a gelatin mixture [29]. The elasticity of the gelatin mixture is used to mimic the human breast tissue is 35 kPa. Silica powder is added to the mixture to simulate the acoustic scattering of human tissue. The flexible needle is made of Nitinol alloy (nickel and titanium). The Nitinol needle has a diameter of 0.5 mm with a bevel angle (at the tip) of 30°.

3. Experiments

3.1. Experimental Plan

Experiments are conducted to validate the proposed tracking, path planning and steering algorithms. The complete system is evaluated by steering the needle towards a target while avoiding an obstacle. The final needle tip position is evaluated in order to determine the targeting accuracy. The targeting accuracy represent the goal of needle steering which is reaching a certain position in 3D space while avoiding an obstacle (by following the optimal path) (Fig. 8). The experiments are conducted to estimate the system accuracy by applying different insertion scenarios. Three experimental cases are performed to validate the proposed control system. Each case is performed five times.

- In Case I, the needle is steered to avoid a virtual obstacle and reach a virtual target at a specific location.
- In Case II, the needle is steered to avoid a virtual obstacle and reach a moving virtual target (size 2.0 mm).
- In Case III, the needle is steered to avoid a moving virtual obstacle and reach a moving virtual target (size 2.0 mm).

The proposed virtual obstacle has a cylindrical shape (e.g., blood vessel) with a 20 mm diameter. The obstacle location is set to (60/4/0) mm in the $(x/y/z)$-axes (frame (Ψ_0)). Obstacle motion is simulated in Case III. At needle insertion, the obstacle is moved with a velocity of 0.3 mm/s in the negative y-axis (frame (Ψ_0)) for a period of 10 seconds. The simulated obstacle motion is used to evaluate the tolerance in a dynamic environment, where blood vessels, bones and vital organs constantly move. The target

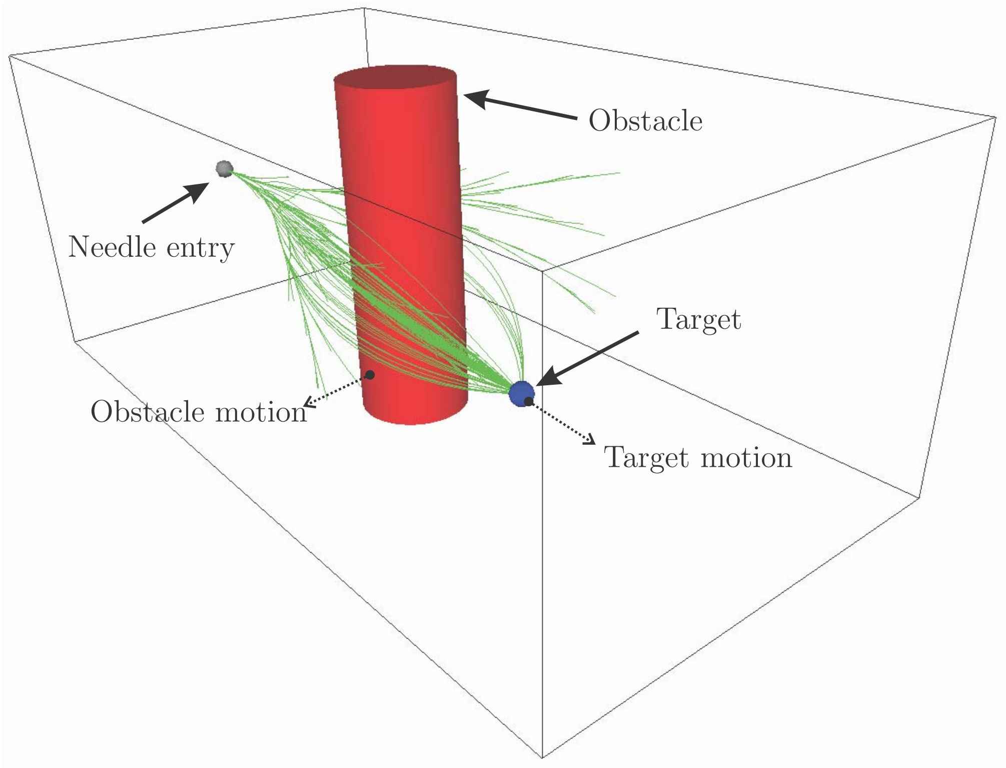

Figure 8: Experimental needle steering scenario: The needle tip pose is tracked using an ultrasound transducer (Fig 7). A cylindrical-shaped obstacle (blood vessel) is placed in the direct path of the needle to reach a spherical target. Needle paths are computed (green lines) using a customized sampling-based rapidly exploring random trees motion planner. The feasible needle paths are selected, and an optimal path is chosen which maximizes the clearance from the obstacle. The needle is steered along the chosen path. During the various experimental cases, the needle path is replanned online in order to compensate for the virtual obstacle and target motion.

location is set to (100/-10/-10) mm in the $(x/y/z)$-axes (frame (Ψ_0)). Target motion is simulated in Cases II and III. After 20 seconds of needle insertion, the target is moved with a velocity of 0.4 mm/s in the positive x-axis (frame (Ψ_0)) until the target is reached. The simulated target motion results in a clinically relevant displacement of approximately 7.0 mm [8, 1]. Target motion is simulated in order to evaluate the effects of the exerted force from the needle on a real target, causing target motion.

Table 1: Targeting errors in ultrasound needle steering are presented (Cases I-III). Mean absolute errors and standard deviations for needle tip targeting along x- (ϵ_x), y- (ϵ_y) and z- (ϵ_z) (frame (Ψ_0)) are provided. The Root Mean Square (RMS) errors and standard deviations in targeting accuracy are evaluated. Each experiment is repeated five times.

Case	ϵ_x [mm]	ϵ_y [mm]	ϵ_z [mm]	RMS [mm]
I	0.05±0.04	1.92±0.83	1.92±0.62	2.78±0.76
II	0.04±0.03	1.30±0.58	0.87±0.50	1.66±0.46
III	0.04±0.03	2.89±0.65	1.67±0.68	3.45±0.25

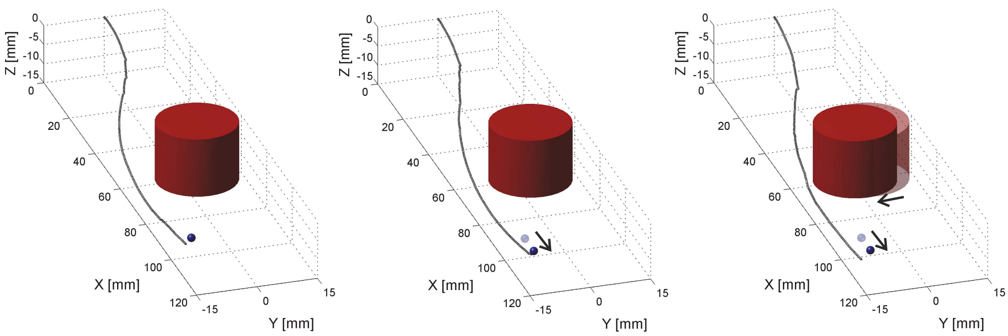

(a) (b) (c)

Figure 9: Representative experimental needle steering results and Root Mean Square (RMS) targeting errors: (a) Case I (no obstacle or target motion) - RMS error: 2.78 mm. (b) Case II (only target motion) - RMS error: 1.66 mm. (c) Case III (both obstacle and target motion) - RMS error: 3.45 mm. The initial position of the cylindrical obstacle (blood vessel) is shaded red, while its end position is solid red. The shaded blue sphere represents the initial target location, while the final target locations is represented by a solid blue sphere.

3.2. Experimental Results

The results from experiments in Case I, II and III are provide in Table 1. A single representative experiment of Cases I, II and II are shown in Fig. 9(a), (b) and (c), respectively. After the needle is steered to reach the target, its final needle tip location is evaluated with respect to the target location. The mean absolute errors with standard deviations of the needle tip along x- (ϵ_x), y- (ϵ_y) and z- (ϵ_z) (frame (Ψ_0)) are reported. The Root Mean Square (RMS) errors are determined in order to evaluate the distance to target. In Case I where both obstacle and target are stationary, a targeting error of 2.78 mm is reported. For Case II where a stationary obstacle is combined with a moving target, a targeting error of 1.66 mm is reported. In Case III where both obstacle and target motion is simulated, a targeting error of 3.45 mm is reported.

3.3. Discussion

By comparing Cases I and II, it is observed that the results of Case II in which target motion is simulated, better targeting accuracy is achieved. Further, by observing Case III, it is expected, that obstacle motion in this specific scenario does not influence the targeting accuracy, because of the planner criteria which maximizes the distance to obstacles. Since the maximum distance to obstacle is already reached, the available tolerance between planned path and obstacle is shown. Thus, by comparing Cases II and III, in which both target motion is simulated, similar targeting accuracies are expected. Given the differences in targeting accuracies between Cases II and III, and the similar targeting accuracies in Cases I and III, it can also be ruled out that target motion effects the targeting accuracy. It is more likely that external factors like soft-tissue simulant elasticity influence needle steering, since the experiments are conducted in different soft-tissue simulants. Variations in the soft-tissue simulant elasticity influences the expected needle curvature, which influences needle planning and steering.

4. Conclusions and Future Work

In this study, three-dimensional needle tip tracking and steering using two-dimensional (2D) ultrasound is presented. Needle tip tracking is achieved by a 2D ultrasound transducer which is orientated perpendicular to the direction of needle insertion. The transducer is moved during needle insertion according to needle tip motion. This allows for the needle tip pose to be computed. The computed needle tip pose is used to determine possible motion plans for the needle to reach a target while avoiding obstacles. In this research, the optimal trajectory is chosen by using a criteria that maximizes the distance to obstacles. The needle is steered along the optimal trajectory using duty cycled spinning of the needle. During needle insertion replanning is used to compensate for perturbation in needle steering, and to consider obstacle and target motion. The presented work in this study shows the feasibility of ultrasound needle steering which considers obstacle and target motion. Experiments show maximum targeting errors of 3.45 mm (RMS) in cases where obstacle and target motion is simulated.

For future work, we will investigate the effects of perturbation in needle steering. Since the predicted needle tip pose is used in replanning, large perturbation in needle steering causes in accurate motion plans to be computed. It is therefore required to investigate the sensitivity to perturbation in needle steering. Further, more testing scenarios will be applied to investigate robustness and to evaluate targeting accuracy of the proposed needle steering system.

References

[1] M. Abayazid, J. Buijs, op den, C. Korte, de, and S. Misra, "Effect of skin thickness on target motion during needle insertion into soft-tissue phantoms," in *Proceedings of the IEEE RAS/EMBS International Conference on Biomedical Robotics and Biomechatronics (BioRob)*. Rome, Italy, June 2012, pp. 755–760.

[2] N. Abolhassani, R. V. Patel, and M. Moallem, "Needle insertion into soft tissue: A survey," *Medical Engineering and Physics*, vol. 29, no. 4, pp. 413–431, 2007.

[3] J. E. Aldrich, "Basic physics of ultrasound imaging," *Critical Care Medicine*, vol. 35, no. 5, pp. S131–S137, 2007.

[4] R. Alterovitz, M. Branicky, and K. Goldberg, "Motion planning under uncertainty for image-guided medical needle steering," *The International journal of robotics research (IJRR)*, vol. 27, no. 11-12, pp. 1361–1374, 2008.

[5] R. Alterovitz, A. Lim, K. Goldberg, G. S. Chirikjian, and A. M. Okamura, "Steering flexible needles under markov motion uncertainty," in *Proceedings of the IEEE International Conference on Intelligent Robots and Systems (IROS)*. Alberta, Canada, August 2005, pp. 1570 – 1575.

[6] Y. Bar-Shalom, X. R. Li, and T. Kirubarajan, *Estimation with Applications to Tracking and Navigation*. New York, USA: John Wiley & Sons., 2001.

[7] N. J. Cowan, K. Goldberg, G. S. Chirikjian, G. Fichtinger, K. B. Reed, V. Kallem, W. Park, S. Misra, and A. M. Okamura, *Surgical Robotics*. Springer US, 2011, ch. Robotic Needle Steering: Design, Modeling, Planning, and Image Guidance, pp. 557–582.

[8] E. E. Deurloo, K. G. Gilhuijs, L. J. S. Kool, and S. H. Muller, "Displacement of breast tissue and needle deviations during stereotactic procedures," *Investigative Radiology*, vol. 36, no. 6, pp. 347–353, 2001.

[9] S. P. DiMaio and S. E. Salcudean, "Needle steering and model-based trajectory planning," in *Proceedings of the International Conference on Medical Image Computing and Computer-Assisted Intervention (MICCAI)*, vol. 2878. Montral, Canada, November 2003, pp. 33–40.

[10] S. P. DiMaio, E. Samset, G. Fischer, I. Iordachita, G. Fichtinger, F. Jolesz, and C. M. Tempany, "Dynamic mri scan plane control for passive tracking of instruments and devices," in *Proceedings of the 10th international conference on Medical image computing and computer-assisted intervention.* Brisbane, Australia, October 2007, pp. 50–58.

[11] V. Duindam, R. Alterovitz, S. Sastry, and K. Goldberg, "Screw-based motion planning for bevel-tip flexible needles in 3d environments with obstacles," in *Proceedings of the IEEE International Conference on Robotics and Automation (ICRA).* Pasadena, CA, USA, May 2008, pp. 2483–2488.

[12] V. Duindam, J. Xu, R. Alterovitz, S. Sastry, and K. Goldberg, "Three-dimensional motion planning algorithms for steerable needles using inverse kinematics," *The International Journal of Robotics Research*, vol. 29, no. 7, pp. 789–800, 2010.

[13] J. A. Engh, G. Podnar, S. Y. Khoo, and C. N. Riviere, "Flexible needle steering system for percutaneous access to deep zones of the brain," in *Proceedings of the IEEE Annual Northeast Bioengineering Conference (NEBEC).* Easton, Pennsylvania, USA, April 2006, pp. 103–104.

[14] H. Fred, "Drawbacks and limitations of computed tomography: views from a medical educator," *Texas Heart Institute Journal*, vol. 31, no. 4, pp. 345–348, 2004.

[15] N. D. Glossop, K. Cleary, L. Kull, and F. Banovac, "Needle tracking using the aurora magnetic position sensor," in *Proceedings Computer Assisted Orthopaedic Surgery.* Santa Fe, USA, June 2002, pp. 90–92.

[16] D. Glozman and M. Shoham, "Image-guided robotic flexible needle steering," *IEEE Transactions on Robotics*, vol. 23, no. 3, pp. 459–467, 2007.

[17] A. Grant and J. Neuberger, "Guidelines on the use of liver biopsy in clinical practice," *Journal of Gastroenterlogoly and Hepatology*, vol. 45, no. Supplement IV, pp. IV1–IV11, 1999.

[18] K. Hauser, R. Alterovitz, N. Chentanez, A. Okamura, and K. Goldberg, "Feedback control for steering needles through 3d deformable tissue using helical paths," in *Proceedings of Robotics: Science and Systems (RSS)*, vol. 37. Seattle, USA, June 2009.

[19] J. Huang, J. Triedman, N. Vasilyev, Y. Suematsu, R. Cleveland, and P. Dupont, "Imaging artifacts of medical instruments in ultrasound-guided interventions," *Journal of Ultrasound in Medicine*, vol. 26, no. 10, pp. 1303–1322, 2007.

[20] V. Kallem and N. Cowan, "Image-guided control of flexible bevel-tip needles," in *Proceedings of the IEEE International Conference on Robotics and Automation (ICRA)*, April 2007, pp. 3015 –3020.

[21] S. M. LaValle, *Planning Algorithms*. Cambridge University Press, 2006, Available at http://planning.cs.uiuc.edu.

[22] D. S. Minhas, J. A. Engh, M. M. Fenske, and C. N. Riviere, "Modeling of needle steering via duty-cycled spinning," in *Proceedings of the IEEE International Conference on Engineering in Medicine and Biology Society (EMBC)*. Lyon, France, August 2007, pp. 2756–2759.

[23] S. Misra, K. B. Reed, B. W. Schafer, K. T. Ramesh, and A. M. Okamura, "Mechanics of flexible needles robotically steered through soft tissue," *International Journal of Robotic Research*, vol. 29, no. 13, pp. 1640–1660, 2010.

[24] Z. Neubach and M. Shoham, "Ultrasound-guided robot for flexible needle steering," *IEEE Transactions on Biomedical Engineering*, vol. 57, no. 4, pp. 799–805, 2010.

[25] P. M. Novotny, J. A. Stoll, N. V. Vasilyev, P. J. del Nido, P. E. Dupont, T. E. Zickler, and R. D. Howe, "Gpu based real-time

instrument tracking with three-dimensional ultrasound," *Medical Image Analysis*, vol. 11, no. 5, pp. 458–464, 2007. [Online]. Available: http://www.sciencedirect.com/science/article/pii/S1361841507000631

[26] W. Park, Y. Wang, and G. Chirikjian, "The path-of-probability algorithm for steering and feedback control of flexible needles," *The International Journal of Robotics Research*, vol. 29, no. 7, pp. 813–830, 2010.

[27] S. Patil and R. Alterovitz, "Interactive motion planning for steerable needles in 3d environments with obstacles," in *Proceedings of IEEE RAS and EMBS International Conference on Biomedical Robotics and Biomechatronics (BioRob)*, September 2010, pp. 893–899.

[28] K. B. Reed, A. Majewicz, V. Kallem, R. Alterovitz, K. Goldberg, N. J. Cowan, and A. M. Okamura, "Robot-assisted needle steering," *IEEE Robotics Automation Magazine*, vol. 18, no. 4, pp. 35 –46, 2011.

[29] R. J. Roesthuis, Y. R. J. van Veen, A. Jayha, and S. Misra, "Mechanics of needle-tissue interaction," in *Proceedings of the IEEE International Conference on Intelligent Robots and Systems (IROS)*. San Francisco, California, USA, September 2011, pp. 2557–2563.

[30] A. Shkolnik, M. Walter, and R. Tedrake, "Reachability-guided sampling for planning under differential constraints," in *Proceeding of the IEEE International Conference on Robotics and Automation (ICRA)*, May 2009, pp. 2859–2865.

[31] G. Taubin, "Estimation of planar curves, surfaces, and nonplanar space curves defined by implicit equations with applications to edge and range image segmentation," *IEEE Transactions on Pattern Analysis and Machine Intelligence*, vol. 13, no. 11, pp. 1115–1138, 1991.

[32] Y. R. J. van Veen, A. Jahya, and S. Misra, "Macroscopic and microscopic observations of needle insertion into gels," *Proceedings of the Institution of Mechanical Engineers, Part H: Journal of Engineering in Medicine*, vol. 226, no. 6, pp. 441–449, June 2012.

[33] R. J. Webster, J. S. Kim, N. J. Cowan, G. S. Chirikjian, and A. M. Okamura, "Nonholonomic modeling of needle steering," *International Journal of Robotics Research*, vol. 25, no. 5-6, pp. 509–525, 2006.

[34] J. Xu, V. Duindam, R. Alterovitz, and K. Goldberg, “Motion planning for steerable needles in 3d environments with obstacles using rapidly-exploring random trees and backchaining,” in *Proceedings of the IEEE International Conference on Automation Science and Engineering (CASE)*, August 2008, pp. 41–46.

Conclusions

In this study, it is shown that three-dimensional needle tip tracking using two-dimensional (2D) ultrasound is possible. This is accomplished by orientating the 2D transducer perpendicular to the needle insertion direction and position it at the needle tip. The required motion of the ultrasound transducer during insertion is determined by correcting the needle insertion velocity by tip velocities. A positioning device is used to reposition the ultrasound transducer during insertion to provide pose feedback of the needle tip. It is shown that needle tip tracking is achieved with maximum tracking errors in tip positions along x-, y- and z-axes of 0.64 mm, 0.25 mm and 0.27 mm, respectively. The maximum reported orientation errors about y-, and z-axes are $2.68°$ and $2.83°$, respectively.

The proposed method to determine the needle tip pose using ultrasound needle tracking is used in path planning and needle steering. The needle tip pose is used in path planning to compute feasible trajectories to reach a target while avoiding obstacles. In this study, the optimal trajectory is determined by using a criteria which maximizes the distance to obstacles (maximize safety). The needle is steered along the trajectory using duty cycled needle steering, which relaxes the constraint on constant curvature of the needle. During needle insertion, the planner is updated with the actual needle tip pose, and obstacle and target locations. Replanning allows for compensation of perturbations in needle steering and to demonstrate the steering capabilities with environmental changes like target and obstacle motion. Experiments show a bevel-tipped Nitinol needle with a diameter of 0.5 mm which is successfully maneuvered around a virtual obstacle to reach a virtual target. Maximum targeting error of 3.5 mm (RMS) are shown, where obstacle and target motion is simulated. However, more scenarios should be evaluated to verify if this claim holds.

Recommendations and Future Work

Future work for this project can be divided into two parts: Ultrasound needle tracking, and needle steering. In ultrasound tracking, a linear model combined with Kalman observer is used to reduce noise in the tracking system and to determine the needle tip state evolvement. The linear model used in this study has shortcomings in describing the needle tip motion. The presented linear model can be used to describe the needle tip motion for small needle deflections with sufficient measurement updates. The linear model suffers from inaccurate state predictions in situations where large needle deflections without measurement updates occur. Therefore non-linear models capable of modeling the needle tip motion should be considered. From ultrasound images it is known, that visualization of areas underneath obstacles is limited. By using a non-linear model which takes control inputs into account, accurate state estimation can be provided when the needle maneuvers underneath obstacles (e.g., blood vessels, organs and bones).

Further, improved ultrasound needle tracking can be achieved by additional image processing. The presented image processing algorithm detects the needle in ultrasound images which is affected by the comet tail artifact (CTA). In experiments using biological tissue (chicken breast), image processing showed sensitivity for tissue properties (e.g., tendons) in the immediate vicinity of the needle tip. The contrast between tendon and needle is low which makes it difficult for the proposed method to distinguish between needle and tendon tissue. Therefore alternative techniques to determine the needle location or to distinguish between needle and tendon would be useful and can provide additional robustness. By fusing the results of different image processing techniques, improved needle position feedback can be achieved and measurement noise reduced.

Further, only flat surfaces are allowed in the current proposed ultrasound tracking method. In order to provide more relevant needle tip tracking in clinical applications, needle tracking over curved surface should be considered. This includes the use of force sensors to guarantee contact between transducer and tracking surface.

In needle steering, we will investigate the effects of perturbation in needle steering. Since the predicted needle tip pose is used in replanning, large perturbation in needle steering causes inaccurate motion plans to be computed. It is therefore required to investigate the sensitivity to perturbation in needle steering.

Also alternatives types of needle steering should be considered. Duty cycling depends on the constant curvature of the needle which is dependent on needle and tissue properties. In clinically relevant scenarios tissue properties are commonly unknown, therefore needle steering techniques with less dependency on tissue properties should be considered.

Further, it can be useful to investigate other types of path planning methods to optimally reach a target (e.g., mathematically determined optimal trajectories)

Appendix A: Abstract Submission, Dutch Biomedical Engineering Conference.

THREE-DIMENSIONAL FLEXIBLE NEEDLE STREERING USING TWO-DIMENSIONAL ULTRASOUND IMAGES

G.J. Vrooijink[†]*, M. Abayazid[†], S. Patil[‡], R. Alterovitz[‡] and S. Misra[†]

[†]University of Twente, 7500 AE Enschede, The Netherlands.
E-mail: {g.j.vrooijink, m.abayazid, s.misra}@utwente.nl
[‡]University of North Carolina, Chapel Hill, USA 27599-3175.
E-mail: {sachin, ron}@cs.unc.edu

ABSTRACT

One of the most commonly performed minimally invasive surgical procedures is needle insertion. Such needle insertions are often performed either for diagnosis (e.g., biopsies) or therapy (e.g., brachytherapy), both of which require accurate needle placement. These procedures are frequently performed under ultrasound image-guidance which provides visual feedback. Clinicians usually use rigid bevel-tipped needles that easily cut and penetrate the soft tissue. The use of rigid bevel-tipped needles offer limited steering capabilities. Steering allows for the compensation of target motion, and the initial misalignment between needle and target. Flexible bevel-tipped needles offer steering capabilities to compensate for target motion and initial misalignment. Further, flexible needles can be steered to avoid sensitive organs and obstacles. In order to provide accurate steering, the needle needs to be accurately controlled at its base. Steering a flexible needle in three-dimensional (3D) space is a demanding task, and requires needle visualization throughout the entire insertion.

In this study, 3D needle tip pose is obtained by a novel technique which uses a two-dimensional (2D) ultrasound transducer [1]. The 2D transducer is placed perpendicular to the needle insertion direction (Fig. 1). Position measurement of the needle tip in the out-of-plane direction of the transducer cannot be obtained directly. Therefore, the transducer needs to be positioned at the needle tip during insertion, which is done by a positioning device. Relocation of the transducer is performed using a Kalman observer and compensator. The observer is used to minimize the influence of noise, and to estimate the needle tip position and velocity. The compensator uses the needle insertion velocity corrected by tip velocities to determine the required out-of-plane motion. Locating the transducer at the needle tip during insertion allows for the computation of the tip pose. Experiments show that maximum mean errors in needle tip positions are 0.64 mm, 0.25 mm and 0.27 mm along the x-, y- and z-axes, respectively, while the tip orientation errors are 2.68º and 2.83º about y- and z-axes, respectively. The tip pose is used to steer the flexible needle towards a target while avoiding obstacles.

Steering of a flexible needle at its base such that it moves towards a target avoiding obstacles requires extensive training and experience. This study uses a customized Rapidly-exploring Random Trees (RRTs)-based path planner, to determine feasible trajectories [2]. These trajectories are computed online and consider the constant radius of curvature introduced by the asymmetric distributed forces acting on the bevel tip. The trajectory is determined by optimizing clinically motivated criteria such as minimizing the insertion length to minimize tissue damage, or maximizing the minimum clearance to obstacles to maximize safety. Control of the needle along such a trajectory is done by duty cycled spinning of the needle during insertion. Duty cycling relaxes the constraint on the constant-curvature of the needle trajectory, and allows any needle curvature between straight and the constant radius of curvature. Improved needle steering is achieved by combining visualization with path planning and duty cycling, which offers the clinician better targeting accuracy in minimally invasive procedures.

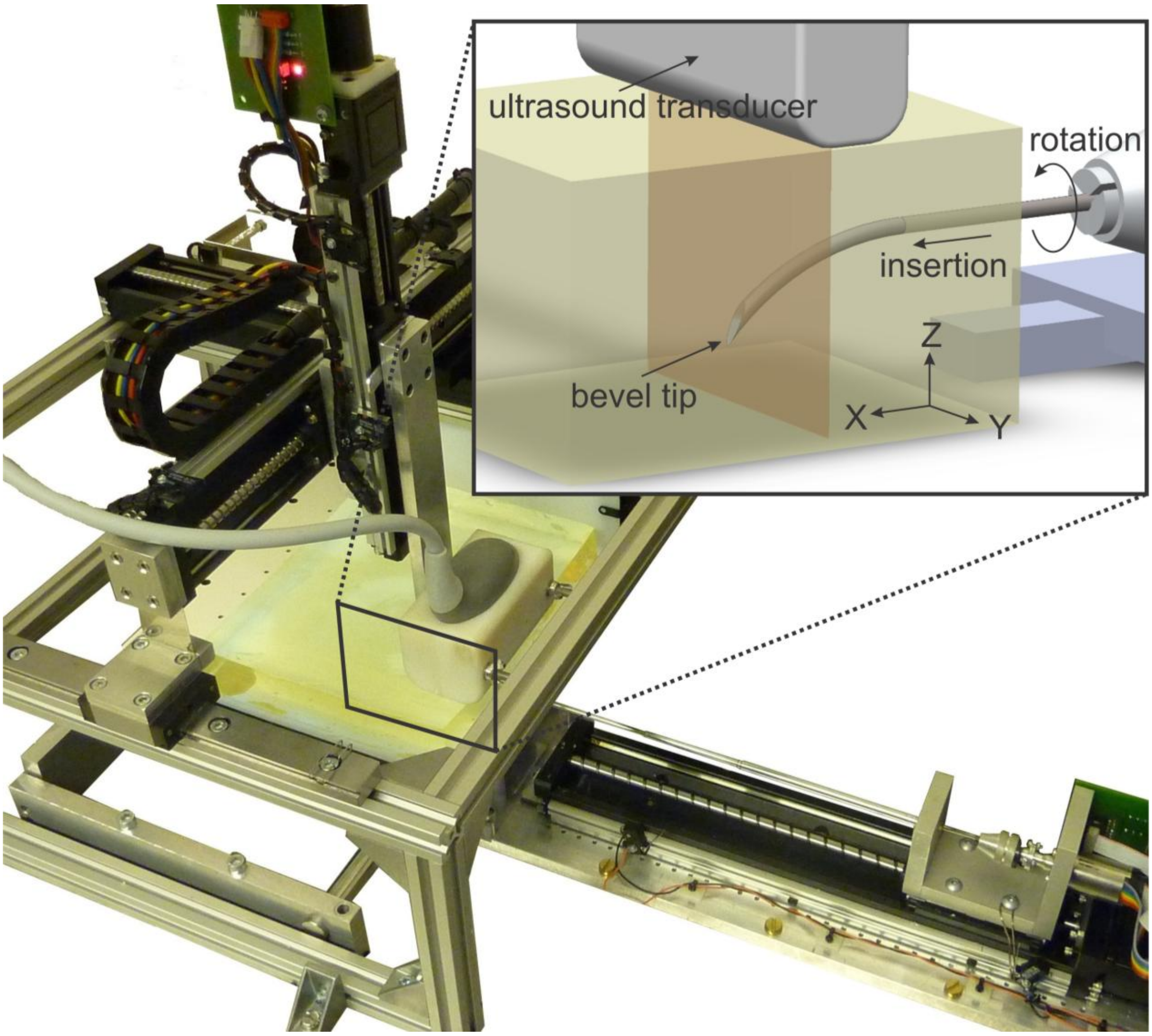

Fig. 1 An overview of the needle tip tracking and steering. A flexible bevel-tipped needle is inserted in the soft-tissue simulant. The soft-tissue simulant is based on a gelatin mixture (by-weight 14.9% gelatin powder, 84.1% water and 1.0% silica) simulating the elasticity property of breast-tissue (35 kPa). During insertion the needle deflects along a curved trajectory in three-dimensional space depending on the orientation of the bevel tip. The needle is tracked by a two-dimensional ultrasound transducer, which is placed perpendicular to the needle insertion direction, as shown in the inset. The transducer provides ultrasound images showing a radial cross-sectional view of the needle. The transducer is robotically repositioned during the insertion in order to provide the needle tip pose. The needle tip pose is used in path planning to steer the needle towards a target while avoiding obstacles.

REFERENCES

[1] G.J. Vrooijink, M. Abayazid and S. Misra. "Real-Time Three-Dimensional Flexible Needle Tracking using Two-Dimensional Ultrasound." In *Proceedings of the IEEE International Conference on Robotics and Automation (ICRA)*, Karlsruhe, Germany, May 2013. (*under review*)

[2] S. Patil and R. Alterovitz. "Interactive Motion Planning for Steerable Needles in 3D Environments with Obstacles." In *Proceedings of the IEEE RAS/EMBS International Conference on Biomedical Robotics and Biomechatronics (BioRob)*, pp. 893-899, Tokyo, Japan, September 2010.

Appendix B: Setup Drawings

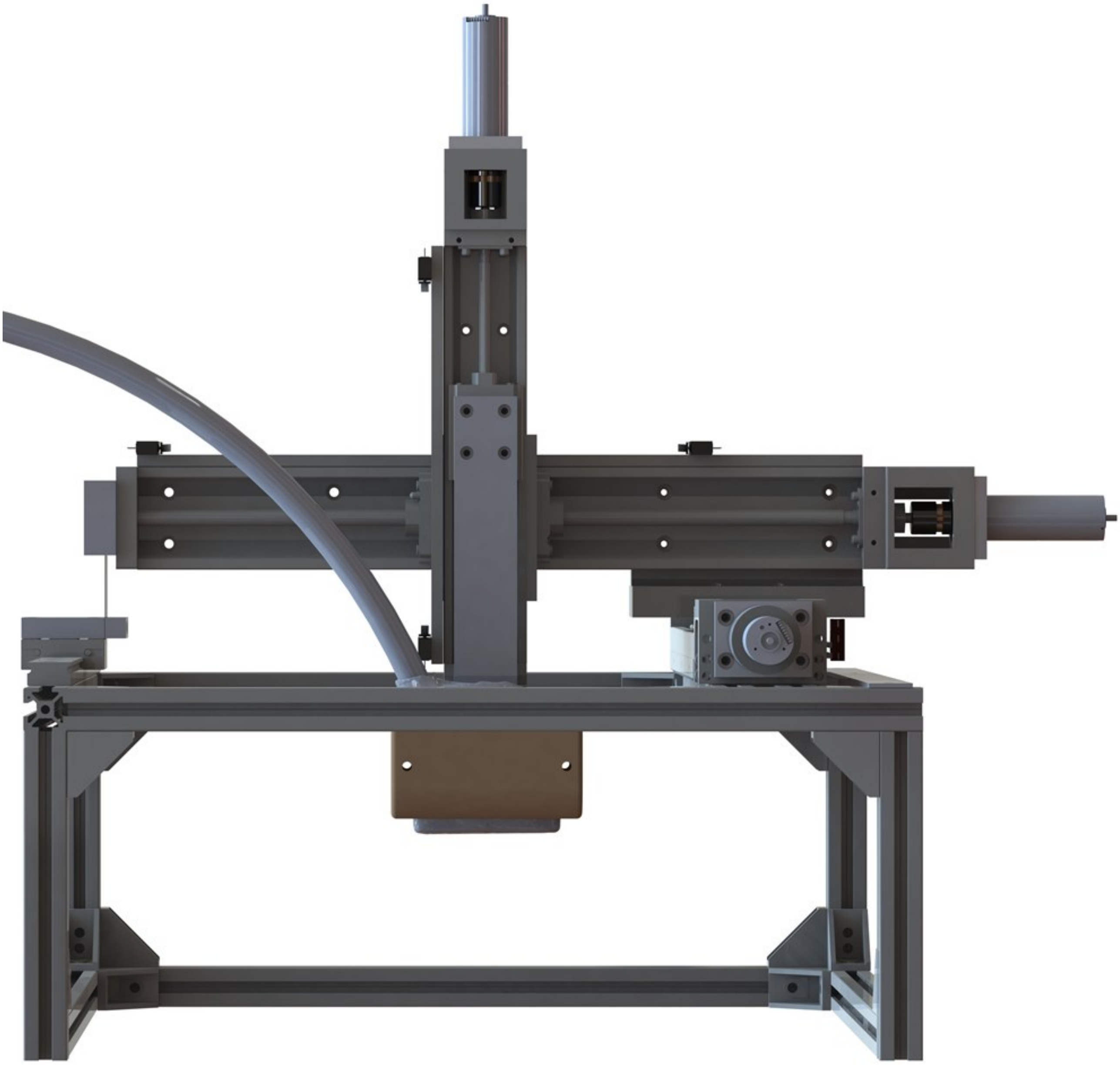

Fig. 1. Solid Works Drawing of the ultrasound positioning device (Front view).

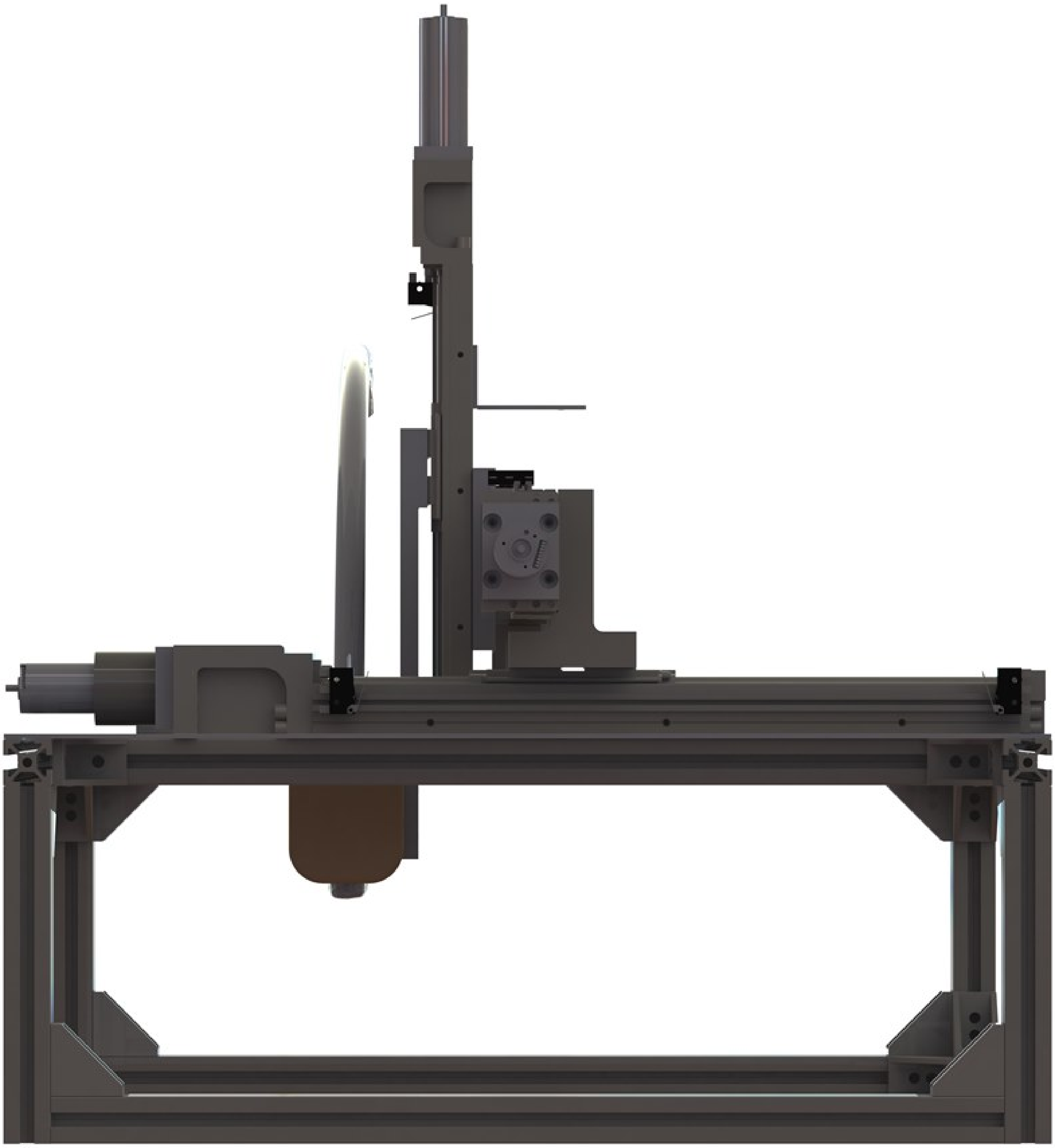

Fig. 2. Solid Works Drawing of the ultrasound positioning device (Side view).

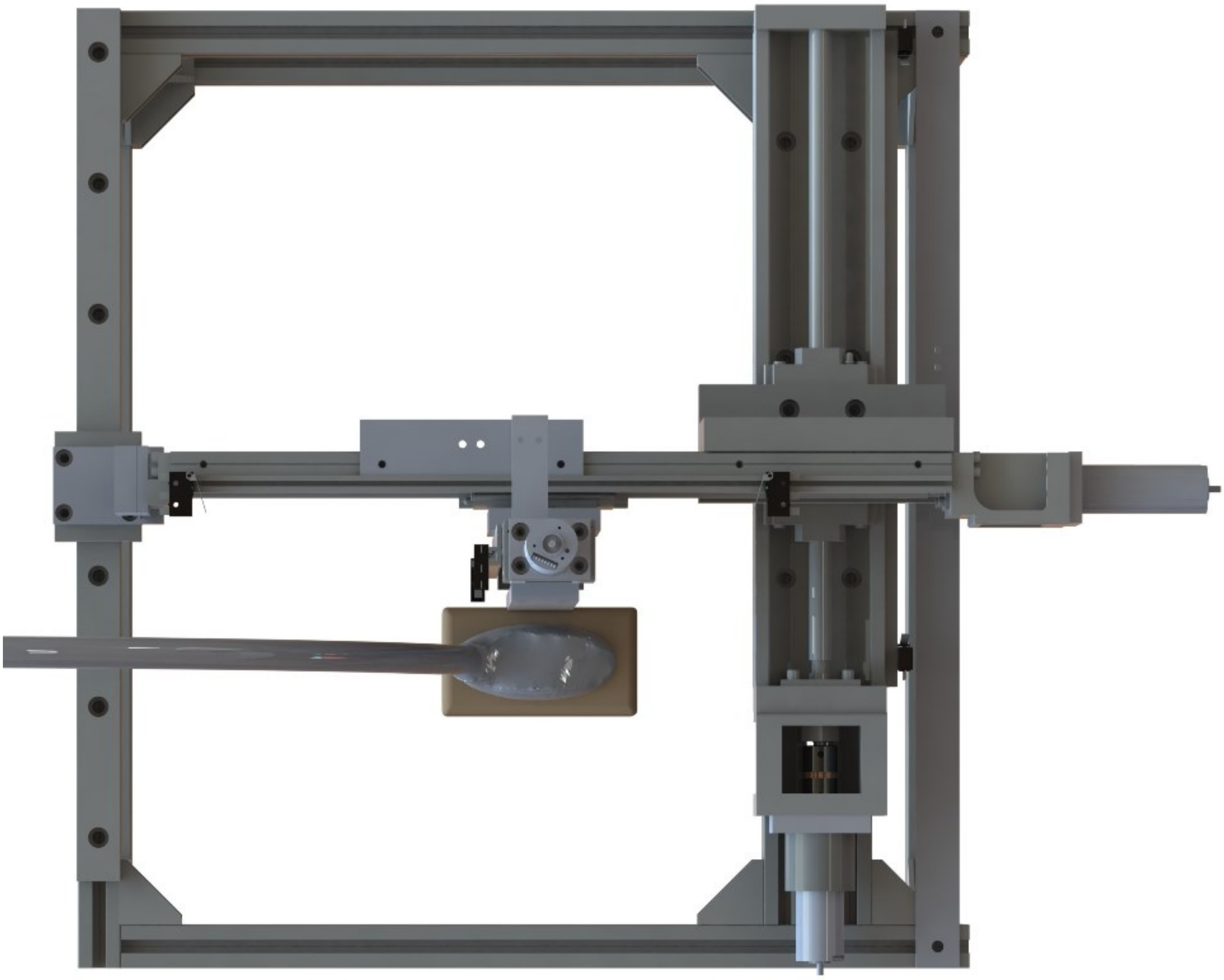

Fig. 3. Solid Works Drawing of the ultrasound positioning device (Top view).

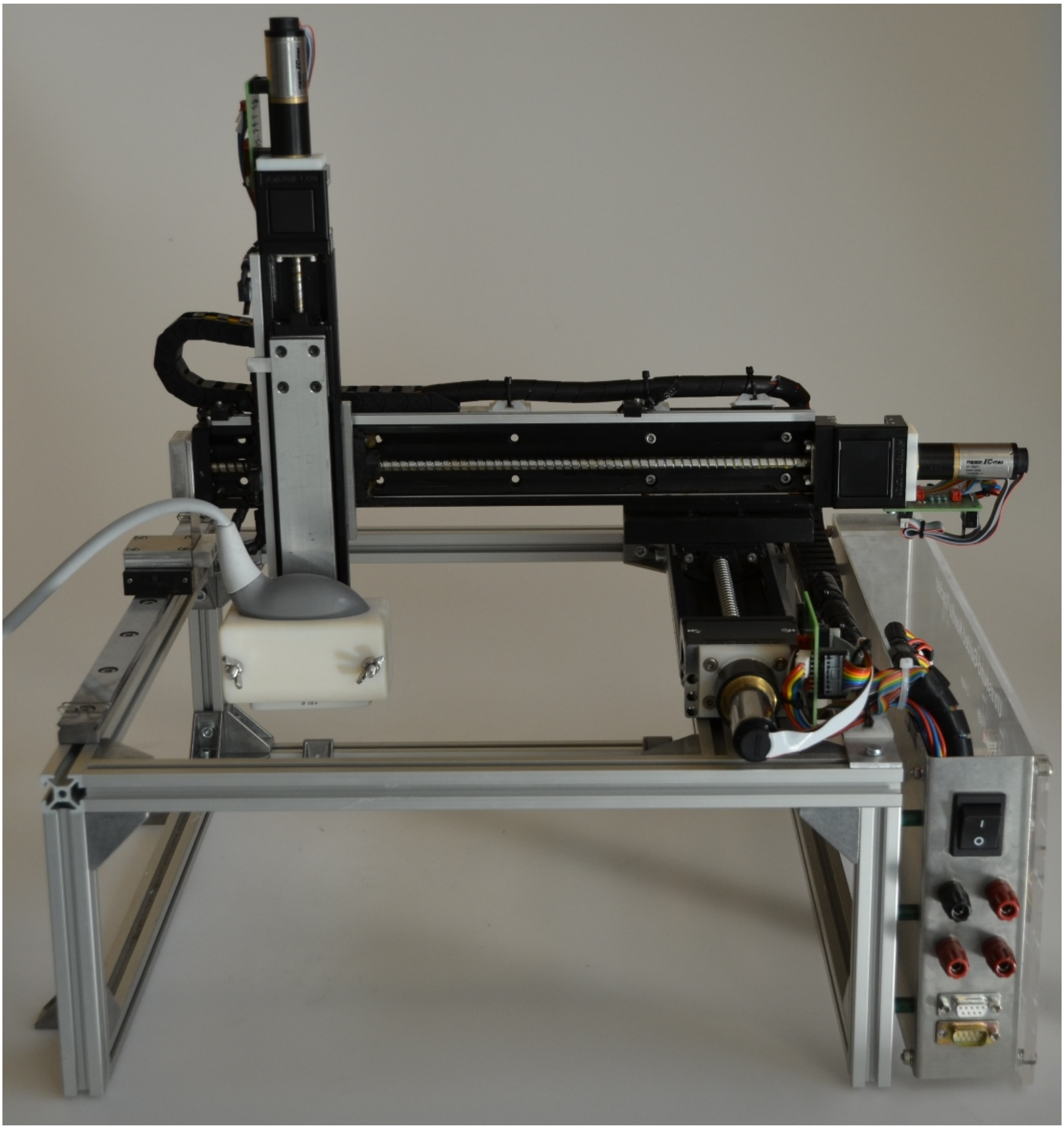

Fig. 4. Picture of the ultrasound positioning device holding the ultasound transducer.

(a) Two-Dimensional (2D) Ultrasound Transducer

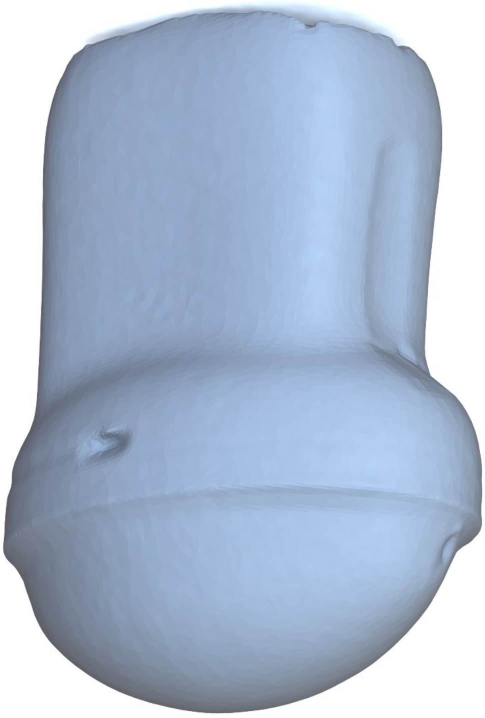

(b) Three-Dimensional (3D) Ultrasound Transducer

Fig. 5. 3D scans of 2D and 3D ultrasound transducer. 3D scans of the ultrasound transducers are made using a Vivid 910 3D laser scanner (Konica Minolta Sensing, Inc., Tokyo, Japan)

(a) Part 1

(b) Part 2

Fig. 6. Two-dimensional (2D) ultrasound transducer clamp. The 2D ultrasound transducer is mounted to the positioning device in a fixed pose using a clamp. (a) Part 1 of the clamp is mounted to the end-effector of the positioning device, while (b) Part 2 of the clamp is used to fix the transducer in Part 1. The designed clamp is 3D printed using a Eden 250 3D printer (Objet Ltd., Rehovot, Israel).

Appendix C: C++ Software

During the project several parts of C++ software have been written. A platform using C++ was build to operate the hardware (e.g., Motor controllers, Ultrasound Machine). Several Classes are written to support:

- CAN Communication
- Elmo Motor Controller
- Needle Insertion Device
- Ultrasound Transducer Positioning Device
- High Resolution Process Timer
- On-line Polynomial Fit
- Ultrasound Image Processing (Needle Comet Tail Artifact Detection)
- Needle Tip Observer (Kalman Observer)
- Needle Tip Tracker
- Duty Cycled Needle Steering
- Data and Video Logging During Experiments
- Three-dimensional Needle Reconstruction in a Volume using Two-Dimensional Ultrasound (Sweep).

Further, a third party path planner was integrated to enable needle steering.

The code has been documented with JavaDoc comments. JavaDoc is a well known documentation standard which is used for documenting Java classes, but can also be used to document C++ software. JavaDoc commenting of the code allows one to auto-generate documentation belonging to the code. The documentation provides the user with knowledge about how the code operates. Further, JavaDoc documentation provides the user with insight of what has been changed between two software versions. The JavaDoc documentation layout is shown below,

```
/**
* Title
*
* Description
*
* @author
* @param
* @return
*/
```

In order to provide version control, a file repository (subversion (SVN)) was created. A branch ultrasound-guided needle steering was created and updated during the project. The experiments performed in Part II are performed with software rev. 103 and 104, while the experiments performed in Part III used software rev. 151. Version control allows one to exactly replicate experiments using the same software conditions.

Appendix D: Kalman Observer

Kalman Observer

In order to improve the position feedback during ultrasound needle tracking, a Kalman observer is added. The Kalman observer is added to minimize the influence of noise in the system and the ability to predict the state ahead [1]. The Kalman observer is explained in Algorithm 1. It is assumed that the needle bends with constant acceleration, therefore the linear model used to predict the state $\mathbf{\hat{x}^-_{k+1|k}}$ and error covariance $\mathbf{P^-_{k+1|k}}$ ahead is given by:

$$\mathbf{\Phi_k} = \begin{bmatrix} \mathbf{I_3} & \Delta t \cdot \mathbf{I_3} \\ \mathbf{0_{3\times 3}} & \mathbf{I_3} \end{bmatrix} \tag{1}$$

where I_3 is a three by three identity matrix, $\mathbf{0_{3\times 3}}$ a three by three matrix filled with zeros and Δt the sampling time. The state vector is given by,

$$\mathbf{\hat{x}_{k|k-1}} = \begin{bmatrix} \mathbf{\hat{p}_k} \\ \hline \mathbf{\Delta\hat{p}_k} \end{bmatrix} \tag{2}$$

where $\mathbf{\hat{p}_k}$ and $\mathbf{\Delta\hat{p}_k}$ are the position and velocity vectors of the needle tip. The $\mathbf{w_k}$ and $\mathbf{v_k}$ represents the process and measurement noises respectively. These noises are assumed to be white Gaussian noise that has zero mean, therefore the covariance matrices are given by,

$$E[\mathbf{w_k}\mathbf{w_k}^\mathbf{T}] = \begin{cases} \mathbf{Q_k} & n = k \\ \mathbf{0} & n \neq k \end{cases} \tag{3}$$

$$E[\mathbf{v_k}\mathbf{v_k}^\mathbf{T}] = \begin{cases} \mathbf{R_k} & n = k \\ \mathbf{0} & n \neq k \end{cases} \tag{4}$$

where the superscript T denotes the transposed matrix. It is stated that the measurement noise $\mathbf{v_k}$ is uncorrelated with the process noise $\mathbf{w_k}$. Due to the lack of prior knowledge on the process and measurement noises, the matrices Q_k and R_k are manual determined to reduce noise in the system. The projection ahead will be corrected and the Kalman gain updated if measurement is available. If the measurement is not available the projection ahead will be used as estimation directly. Without measurement update the uncertainty region of the projection ahead will increase. It is therefore important to minimize the duration of measurement absence. The Kalman gain will be adjusted upon return of measurements according to the projected error covariance ahead. The adapted Kalman gain ensures a quick decrease in estimation error. The output $\mathbf{\hat{x}_{k+1|k}}$ given by the Kalman observer represents the optimized needle tip position feedback. An experiment was performed to demonstrate the reduce in system noise (Fig. 1). The results are shown in Fig. 2. Results show that by using a Kalman observer, the noise in the system is reduced and the ability to determine the subsequent state when measurement is not available is provided.

Algorithm 1 Kalman observer

Require:
$\mathbf{\hat{x}_{k|k-1}}$ Initial state
$\mathbf{P_{k|k-1}}$ Initial error covariance

Predict:
$\mathbf{\hat{x}^-_{k+1|k}} = \mathbf{\Phi_k}\mathbf{\hat{x}_{k|k-1}}$
$\mathbf{P^-_{k+1|k}} = \mathbf{\Phi_k}\mathbf{P_{k|k-1}}\mathbf{\Phi_k}^\mathbf{T} + \mathbf{Q_k}$

Update:
if Measurement available **then**
    $\mathbf{K_k} = \mathbf{P^-_{k+1|k}}\mathbf{H^T}[\mathbf{H}\mathbf{P^-_{k+1|k}}\mathbf{H^T} + \mathbf{R_k}]^{-1}$
    $\mathbf{\hat{x}_{k+1|k}} = \mathbf{\hat{x}^-_{k+1|k}} + \mathbf{K_k}[\mathbf{z_k} - \mathbf{H}\mathbf{\hat{x}_{k|k-1}}]$
    $\mathbf{P_{k+1|k}} = [\mathbf{I} - \mathbf{K_k}\mathbf{H}]\mathbf{P^-_{k+1|k}}$
else
    $\mathbf{\hat{x}_{k+1|k}} = \mathbf{\hat{x}^-_{k+1|k}}$
    $\mathbf{P_{k+1|k}} = \mathbf{P^-_{k+1|k}}$
end if

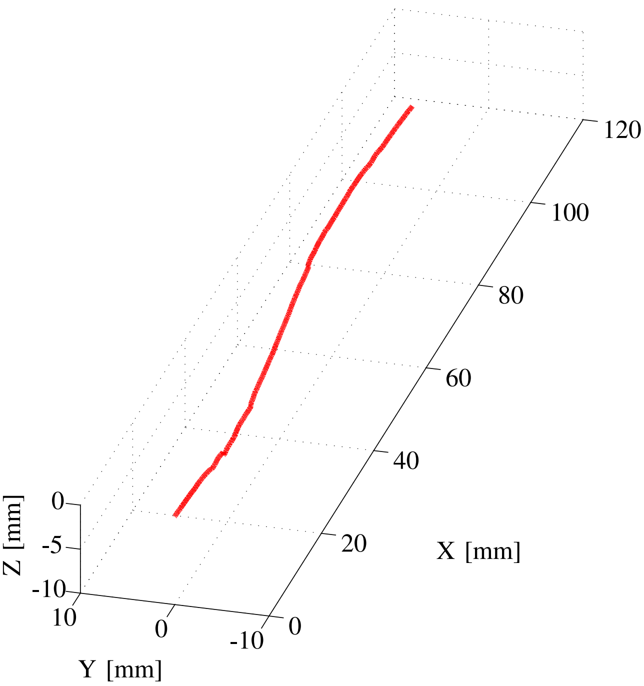

Fig. 1. Three-dimensional needle shape. A bevel-tipped flexible needle is inserted 110 mm and rotated at the same time. During the insertion a full rotation is performed in order to obtain a helical needle shape.

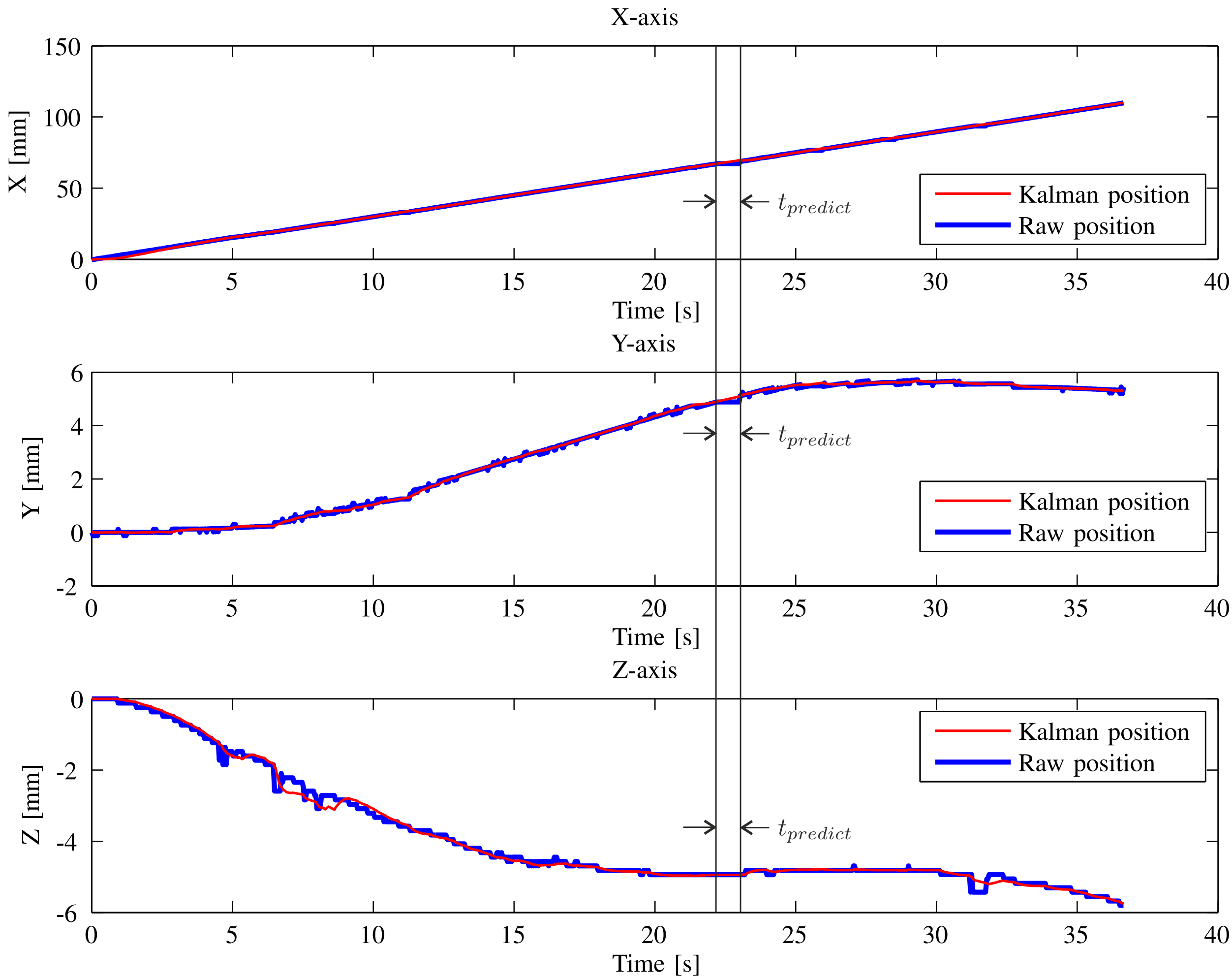

Fig. 2. The position measurements of the needle during insertion. $t_{predict}$ describes a single time interval when no measurement was available and the Kalman observer predicts the subsequent states. The three plots show the needle tip position of the Kalman observer (red) and the raw needle tip position directly determined from image processing (blue).

References

[1] Y. Bar-Shalom, X. R. Li, and T. Kirubarajan, *Estimation with Applications to Tracking and Navigation*. New York, USA: John Wiley & Sons., 2001.